Front. Optoelectron. 2017, 10(4): 329–352
https://doi.org/10.1007/s12200-017-0765-x

REVIEW ARTICLE

Inkjet printing for electroluminescent devices: emissive materials, film formation, and display prototypes

Luhua LAN, Jianhua ZOU, Congbiao JIANG, Benchang LIU, Lei WANG (✉), Junbiao PENG (✉)

Institute of Polymer Optoelectronic Materials and Devices, State Key Laboratory of Luminescent Materials and Devices, South China University of Technology, Guangzhou 510640, China

Abstract Inkjet printing (IJP) is a versatile technique for realizing high-accuracy patterns in a cost-effective manner. It is considered to be one of the most promising candidates to replace the expensive thermal evaporation technique, which is hindered by the difficulty of fabricating low-cost, large electroluminescent devices, such as organic light-emitting diodes (OLEDs) and quantum dot light-emitting diodes (QLEDs). In this invited review, we first introduce the recent progress of some printable emissive materials, including polymers, small molecules, and inorganic colloidal quantum dot emitters in OLEDs and QLEDs. Subsequently, we focus on the key factors that influence film formation. By exploring stable ink formulation, selecting print parameters, and implementing droplet deposition control, a uniform film can be obtained, which in turn improves the device performance. Finally, a series of impressive inkjet-printed OLEDs and QLEDs prototype display panels are summarized, suggesting a promising future for IJP in the fabrication of large and high-resolution flat panel displays.

Keywords inkjet printing (IJP), inks system, film formation, organic light-emitting diodes (OLEDs), quantum dot light-emitting diodes (QLEDs)

1 Introduction

As carriers for the dissemination of information, displays play an important role in creating channels for access to information nowadays. The display industry continues to implement changes and improvements. From the early cathode ray tubes (CRT) to the subsequent liquid crystal displays (LCD) to the new-generation organic light-emitting diodes (OLEDs) and the potential quantum dot light-emitting diodes (QLEDs), display technologies are progressing toward large screen, high resolution, less weight, small thickness, energy saving, and even flexibility [1–5]. Currently, OLEDs have realized industrialization in small and medium sizes and have steadily captured the high-end smartphone market. QLEDs, however, are yet to be commercialized owing to their late invention and research . Several thin film deposition methods such as vacuum evaporation [3,6–8], lithography [9–11], transfer printing [12], spin coating [4,5], and inkjet printing (IJP) [13–15] have been employed to manufacture these multi-layer LED devices. Among them, IJP exhibits the merits of being mask-free, material saving, and compatible with flexible plastic substrates, which is promising for the unprecedented generation of large-scale, low-cost, and flexible displays based on light-emitting diodes.

The working principle of IJP is to eject inks from fine nozzles to a specified position on a treated substrate under the control of a computer, and subsequently, the deposited ink is dried (usually by heating) to evaporate the solvent to form a pre-designed pattern. Generally, the ink droplets are ejected in a continuous or drop-on-demand (DOD) manner (Fig. 1) [16]. In the continuous operating mode (Fig. 1(a)), each droplet ejected from the printed head exhibits uniformity in size and space, which is controlled by the droplet deflection system. First, the droplets are selectively charged by the nozzles. Thereafter, these charged droplets are divided into two parts according to the amount of charge carried under an external applied electric field. Partial droplets involved in the patterning arrive at the specified position on the substrate, whereas other droplets enter the ink recycling system and are carried back to the ink reservoir. Continuous inkjet technology has an advantage over the subsequent DOD mode in terms of printing speed. However, the nozzles based on continuous inkjet technology should be equipped with additional apparatus, such as a droplet charged device, deflection device, and ink recycling system, which result in high cost

Received October 16, 2017; accepted October 25, 2017

E-mails: mslwang@scut.edu.cn, psjbpeng@scut.edu.cn

and low ink utilization ratio. Currently, the DOD mode is the dominant technique for patterning deposition in the manufacture of electronics. In a DOD system (Fig. 1(b)), the generation and ejection of ink droplets are controlled by electrical pulse signals generated by piezoelectric ceramic components. Therefore, ink consumption is substantially reduced in the DOD method. Furthermore, owing to the use of less sophisticated apparatus, the DOD inkjet technique is cost-effective.

Homogeneous films are essential for obtaining high-performance OLEDs and QLEDs. In the inkjet-printed process, the ultimate surface morphologies of patterns are affected by formulation of ink, printing parameters, post treatment, etc. For example, by optimizing the solvent component, the vexing coffee-ring effect can be eliminated. There are still numerous challenges to be overcome to realize the industrialization of inkjet-printed electroluminescent displays.

This review article aims to provide a systematic summary of the major highlights in the realm of OLEDs and QLEDs based on the IJP technique. We will begin with a brief overview of printable emissive materials categorized according to their application in OLEDs and QLEDs devices. Subsequently, several key factors determining the quality of the ultimate printed film are analyzed. We particularly focus on the control of the coffee-ring effect and the strategies of high-resolution pixel arrays by film deposition engineering. The last section of this article will summarize some of the representative pioneering works in the field of OLEDs and QLEDs fabricated via IJP in the past two decades. We anticipate a promising future for IJP in the fabrication of large and high-definition flat panel displays (FPDs).

2 Materials for inkjet printing

Both OLEDs and QLEDs are multilayer-stacked architectures consisting of several organic or inorganic layers. Considering a bottom emission device (Fig. 2) as an example, the functional layers are transparent anode, hole injection layer (HIL), hole transport layer (HTL), emissive layer (EML), electron injection layer (EIL), electron transport layer (ETL), and reflective cathode from bottom to top. Among the materials applied in electroluminescent devices, small molecules and metal electrodes are generally deposited via vacuum evaporation. By contrast, polymers, inorganic nanoparticles (NPs), and nanocrystals are usually dissolved or dispersed in various solvents. They are suitable for solution processing such as spin coating, transfer printing and IJP. There have been several comprehensive review articles regarding transparent electrode materials and organic/inorganic charge transport materials [17–22]. Owing to space limitations, this section will only briefly introduce emissive materials including conjugated polymers, small molecules, and colloidal quantum dots, which are capable of being deposited as EML via IJP.

2.1 Polymers and small-molecular emitters

Since the pioneering work by Friend et al. in 1990, solution-processing polymers as active emitters sandwiched between anodes and cathodes have attracted intense research attention [4]. Many groups have conducted extensive work for developing several kinds of species: polyphenylene vinylene derivatives [23], poly(p-phenylene) derivatives [24], polythiophene derivatives

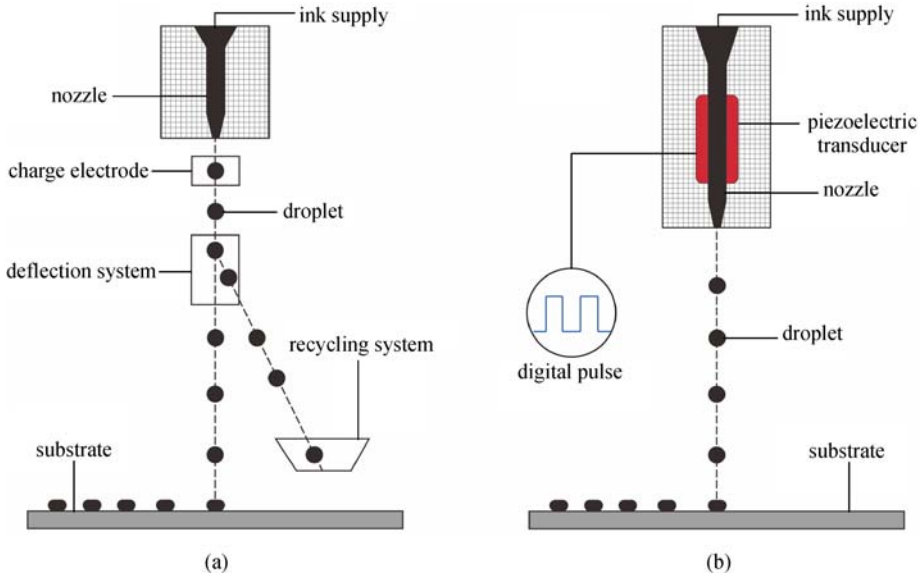

Fig. 1 Schematic diagram of inkjet printing. (a) Continuous mode; (b) DOD mode

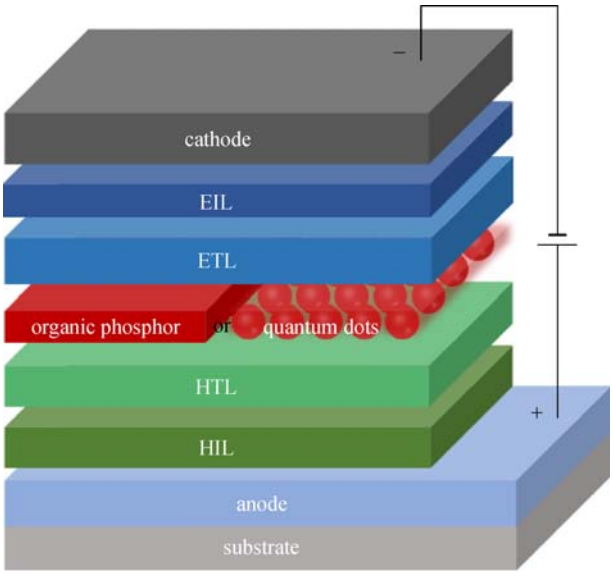

Fig. 2 Multilayer LED device structure

[25], polyfluorene derivatives [26] and partial hyperbranched conjugated polymers [27]. In this context, our laboratory has also carried out investigations for designing and synthesizing efficient phosphors over the past two decades. Combined with the partial work conducted in our laboratory, a series of solution-processable polymers and small molecules that emit tri-phosphor RGB and white visible fluorescence are introduced herein.

Hou et al. [28] used palladium-catalyzed Suzuki coupling reaction to synthesize a series of red-emitting fluorene-based copolymers (PFO-DBT*x*, *x* = 1, 5, 10, 15, 25, 35) by varying the feed ratio of DOF (9,9-dioctylfluorene) and DBT (4,7-di-2-thienyl-2,1,3-benzothiadiazole) (Fig. 3(a)). The emission peaks exhibited tunability in the wavelength range of 628–674 nm with the increase in DBT concentration. In order to obtain green polymer emitters, Guan et al. [29] used the 3,6-carbazole-co-2,6-pyridine segment as the branch and $Ir(ppy)_3$ molecule as the core to synthesize hyperbranched polymers that emit green light via Suzuki polycondensation (Fig. 3(b)). Efficient energy transfer from 3,6-carbazole-co-2,6-pyridine segments to $Ir(ppy)_3$ was observed. Furthermore, such branched structures effectively restrained the interchain interactions and self-quenching of $Ir(ppy)_3$ complexes. Consequently, the peak external quantum efficiency (EQE) and current efficiency (CE) of polymer light-emitting diodes (PLEDs) with this hyperbranched polymer as emitter were 13.3% and 30.1 cd/A, respectively. Recently, Liang et al. [30] synthesized a exciplex-type single greenish-white polymer PFTS comprised of the electron-donating TPA-Cz (4,4′-(9-alkylcarbazole-3,6-diyl)bis-(N,N-diphenylaniline)) in the side chain and the electron-withdrawing SO (dibenzothiophene-5,5-dioxide) unit in the backbone (Fig. 3(c)). The PLEDs based on the polyfluorene derivative PFTS exhibited a remarkable CE of 9.12 cd/A with the CIE (Commission Internationale de L'Eclairage) color coordinate of (0.25, 0.37) [31]. Such white emitting property from a unimolecule provides a strategy to overcome the electroluminescence (EL) instability of blending films.

Compared with polymers, small molecules exhibit the advantages of higher carrier mobility, easier synthesis and purification, and better reproducibility. Therefore, developing low-cost small molecules applicable to solution processing will accelerate the commercialization of printing displays. In 2009, Liu et al. [32] synthesized two kinds of solution-processable small molecule emitters: 2PE-PPF (Fig. 3(d)) and DPE-PPF (Fig. 3(e)) with stable emission and high glass transition temperature (T_g) up to 102°C and 147°C, respectively. Smooth and uniform surface profiles were obtained via spin coating. Li et al. [33] designed asymmetrical 4,7-disubstituted benzothiadiazole derivatives with a carbazolyl moiety opposite to a solubilizing dendron (Fig. 3(f)). A double-layer LED with the architecture of ITO/PEDOT: PSS/PVK (Poly(9-vinylcarbazole))/1a (1b)/Ba/Al exhibited a peak CE of approximately 10.6 cd/A and pure green emission with the color coordinates (0.34, 0.58). These intriguing features enabled them to be deposited as EMLs via IJP. However, small-molecular materials always exhibit the obvious drawback of inferior film quality. They are prone to dewetting and form discontinuous films in the solvent evaporation process. There are two major approaches to improve the film quality of small molecules. One is to design and synthesize molecules with eminent solubility and film formability by increasing the molecular volume and alkyl-chain length [34,35], and the other is to add polymer materials to small molecules to render them conducive to film formation [36,37]. Furthermore, modulating the surface properties of substrates is also a feasible strategy [38].

Both small-molecular OLEDs and PLEDs are hindered by the significant challenge of exploiting highly efficient and stable blue emitters. In this regard, Yang et al. [39–41] designed and synthesized several efficient blue-emitting polyfluorene derivatives with stable emission by linking SO (dibenzothiophene-S,S-dioxide) isomer unit to the PPF (poly[9,9-bis(4-(2-ethylhexyloxy)phenyl)fluorene-2,7-diyl]) skeleton (Fig. 3(g)). They exhibited extreme spectral stability even under varied current density and annealing temperature. Furthermore, the existence of the SO unit facilitated electron injection, which maintained the charge balance when PVK was employed as HTL. The PLEDs based on these polyfluorene derivatives exhibited low turn-on voltage (the voltage when the luminance reaches 1 cd/m^2) of 3.0 V, peak CE of 7.0 cd/A, and peak EQE of 6.4%, which rendered them the most efficient blue PLEDs devices at that time. Zhu et al. [42] reported an asymmetrically 9,10-disubstituted anthracene derivative with good solubility and pure emission (Fig. 3(h)). The peak CE and EQE of this small-molecular blue-emitter-

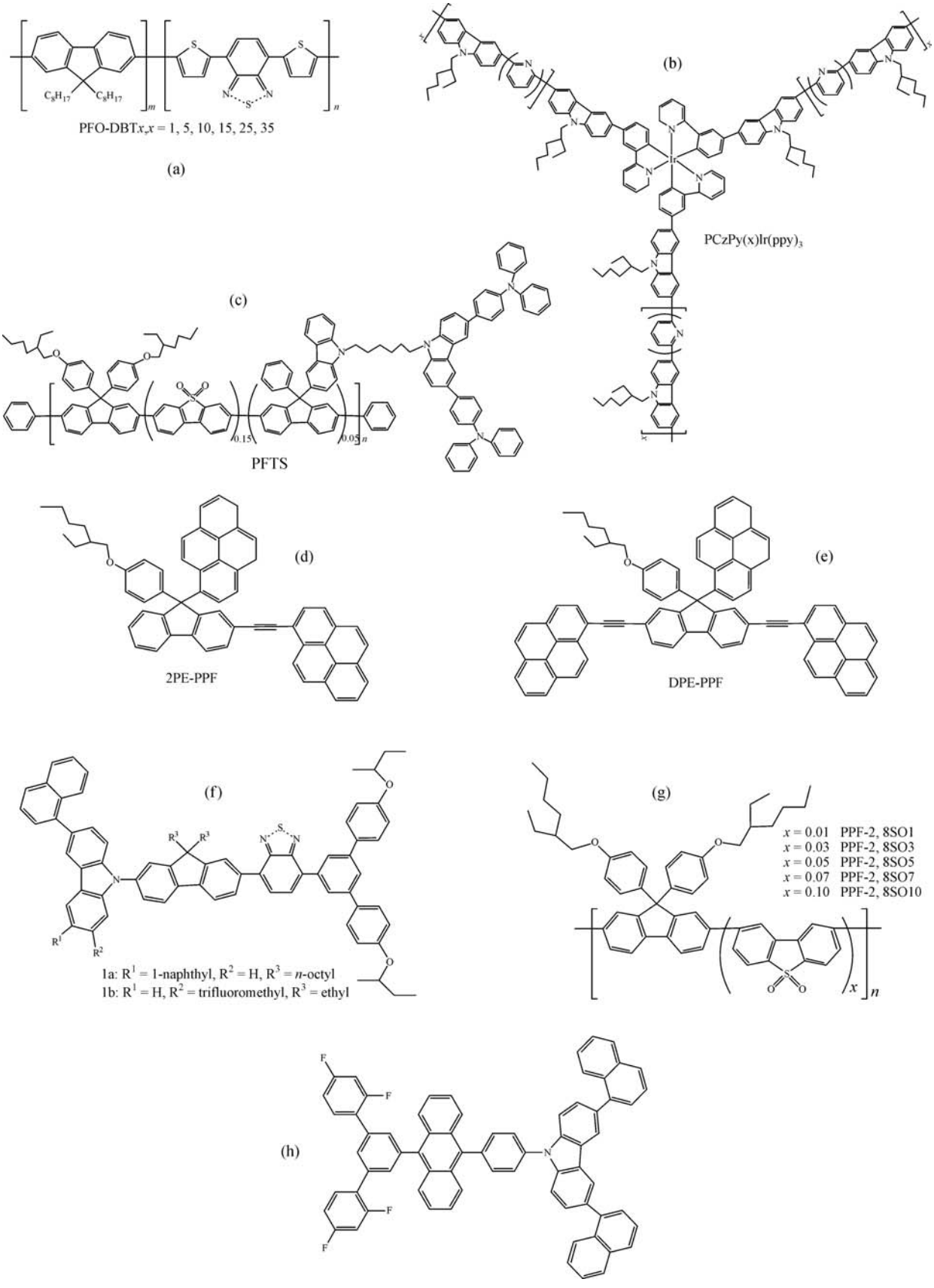

Fig. 3 Chemical structures of the solution-processable emitters

based device could be optimized to 1.88 cd/A and 2.34%, respectively.

2.2 Colloidal quantum dot nanocrystals

Quantum dots (QDs) are morphologically quasi-zero dimension nanoclusters synthesized and dispersed in solution phase. They typically consist of a tiny semiconductor core and a wide bandgap semiconductor shell coating with organic passivating ligands (Fig. 4). Owing to the unique core/shell structure, QDs exhibit surface effect, quantum size effect, and dielectric confinement effect, which lead to outstanding emission properties such as high luminance, narrow full-width-at-half-maximum (FWHM), broad spectrum from ultraviolet (UV) to near-infrared, and tunable spectrum depending on size control [43–46]. This field has attracted increasing interest owing to the immense potential for commercial applications including biological imaging [47,48], LEDs [49–51], photovoltaic devices [52], photoresistors [53], and field-effect transistors [54]. Particularly in the field of LEDs, companies such as Nanoco, Nanosys, QD vision, and NajingTech have been committed to the industrialization of QDs.

Cadmium-based QDs are mainly composed of Cd, Zn, Se, and S. Core/shell CdSe/CdS QDs are sufficiently exploited owing to their high photoluminescence quantum yields (PLQYs), narrow FWHM, and low probability of fluorescence intermittency. Peng et al. [55] demonstrated the synthesis of CdSe/CdS core/shell QDs with zinc-blende structure via the epitaxial growth of proper layers of CdS shell coating onto presynthesized CdSe core. The photoluminescence (PL) decay kinetics and optical properties of these QDs were studied using a time-correlated single-photon counting spectrofluorometer and UV–visible spectrophotometer. The results suggested that the PL lifetime was significantly prolonged up to (16.5±1.0) ns without an apparent blinking phenomenon. Subsequently, Peng et al. developed phase-pure zinc-blende CdSe/CdS QDs and further investigated their ensemble optical properties using single-dot spectroscopy [56]. It was observed that the average "on" time (nonblinking time) accounted for 95%–99%, indicating that such a core/shell structure could effectively suppress PL blinking.

However, cadmium-based QDs contain heavy metal elements, which have destructive effects on human health and ecological environment. Many countries and organizations have issued bans to restrict the use of toxic elements, including cadmium, lead, and mercury in consumer electronics. Therefore, it is imperative to develop high-performance Cd-free QDs to replace recent Cd-based QDs. Accordingly, the promising substitutes that have been exploited at the preliminary stage include perovskite QDs [57–60], InP [61,62], $CuInS_2$ [63,64], doped ZnS/ZnSe (Mn^{2+}, Cu^{2+}) [65,66], silicon QDs [67,68], and carbon QDs (CQDs) [69,70].

Furthermore, perovskite QDs have made remarkable progress in PLQY, which is demonstrated by the increase of the EQEs of the corresponding LEDs devices from 0.76% [57] to 11.7% [60] in the past few years. Song et al. [71] reported all-inorganic perovskite $CsPbX_3$ (X = Cl, Br, I) nanocrystals with outstanding features such as well-dispersed, high PLQYs (> 85%), and tunable and sharp emission (FWHM < 30 nm). Although the device performance was unsatisfactory, the synthesized materials opened a new avenue for display applications. Wang et al. [60] demonstrated the synthesis of self-organized perovskite multiple quantum wells (MQWs). The MQW-based LED demonstrated excellent EQE up to 11.7%. This recording efficiency was attributed to the lower energy gaps, which determine electroluminescence, were well confined by MQWs with higher bandgap, leading to highly efficient radiative decay. Similar to Cd-based QD materials, perovskite QDs with high PLQYs cannot eliminate toxic lead elements. Some researchers have attempted to replace Pb with nontoxic Sn, Bi, Ge, and Cu, but their instability under ambient conditions and poor PL performance are difficult to circumvent [72–75]. In the case of the other Cd-free QD species, both PLQY and PL stability

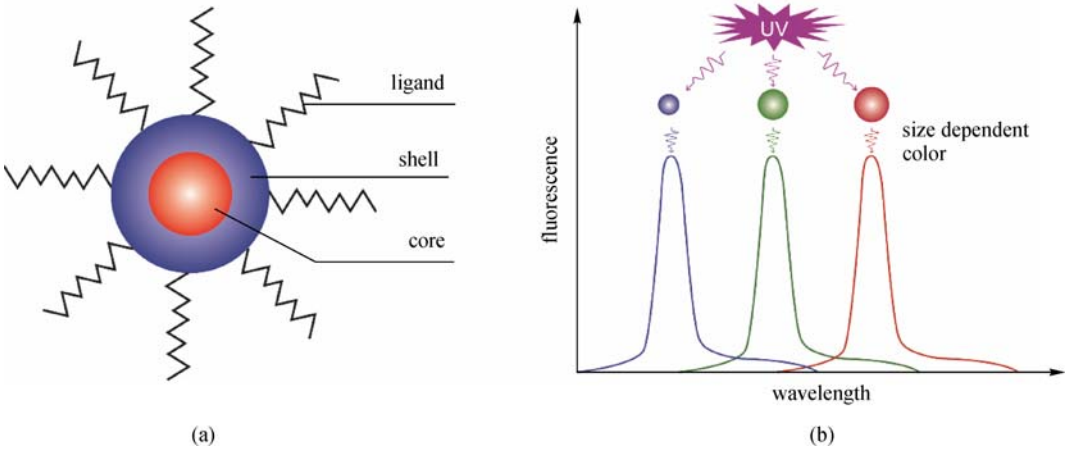

Fig. 4 (a) Quantum dots with core/shell structure; (b) PL spectra of QDs with different size under UV light

are also far worse than those of the CdSe QD species. However, it is expected that the previous huge gap between Cd-based QLEDs and Cd-free QLEDs will continually narrow down owing to industry support. Bai et al. [64] demonstrated the synthesis of low-toxic $CuInS_2$/ZnS coating with hydroxyl-terminated ligands via in situ ligand exchange. Compared to the QLED devices with oleic-acid-capped $CuInS_2$/ZnS QD, the peak brightness and EQE of this hydroxyl-terminated QD-based QLED were enhanced from 338 cd/m^2 and 0.85% to 8375 cd/m^2 and 3.22%, respectively. Yuan et al. [70] recently reported a series of CQDs that demonstrated extraordinary capacity for emitting light covering the entire visible spectrum with PLQY up to 75% for blue CQDs by using a facile solvothermal reaction between citric acid and diamino-naphthalene (Fig. 5). White quantum dot light-emitting diodes (WQLEDs) were fabricated using these RGB CQDs and their CIE color coordinates were located at (0.30, 0.33), which is close to that of the standard illuminant. Furthermore, their peak luminance and CE reached approximately 2050 cd/m^2 and 1.1 cd/A, respectively, which were comparable to those of the WQLEDs based on Cd-based QDs [77,78].

Understanding the quenching mechanism is necessary to design high-performance QDs. In the packed QD layers, the possible decay channels include radiative recombination to emit photons, intragap-state-assisted non-radiative recombination, energy transfer to adjacent QDs or charge transport layers, exciton disassociation through interfacial charge transfer, and Auger recombination [79]. The unfavorable non-radiative channels are remarkably suppressed by controlling the shell composition and density of surface ligands. In this regard, alloying QD with a composition gradient shell is an effective strategy to suppress the nonradiative channels. For example, Lee et al. [76] synthesized 12.7-nm-sized green CdSe/ZnS/ZnS QDs possessing a thick composition-gradient ZnS outer shell. Compared to the smaller green CdSe/ZnS QDs without an added 1.6-nm ZnS outer shell, CdSe/ZnS/ZnS QDs exhibited a twofold increase in PLQYs and longer PL lifetimes whether they were in the form of solution phase or solid film (Fig. 5(c)–5(e)). The peak CE and EQE of the

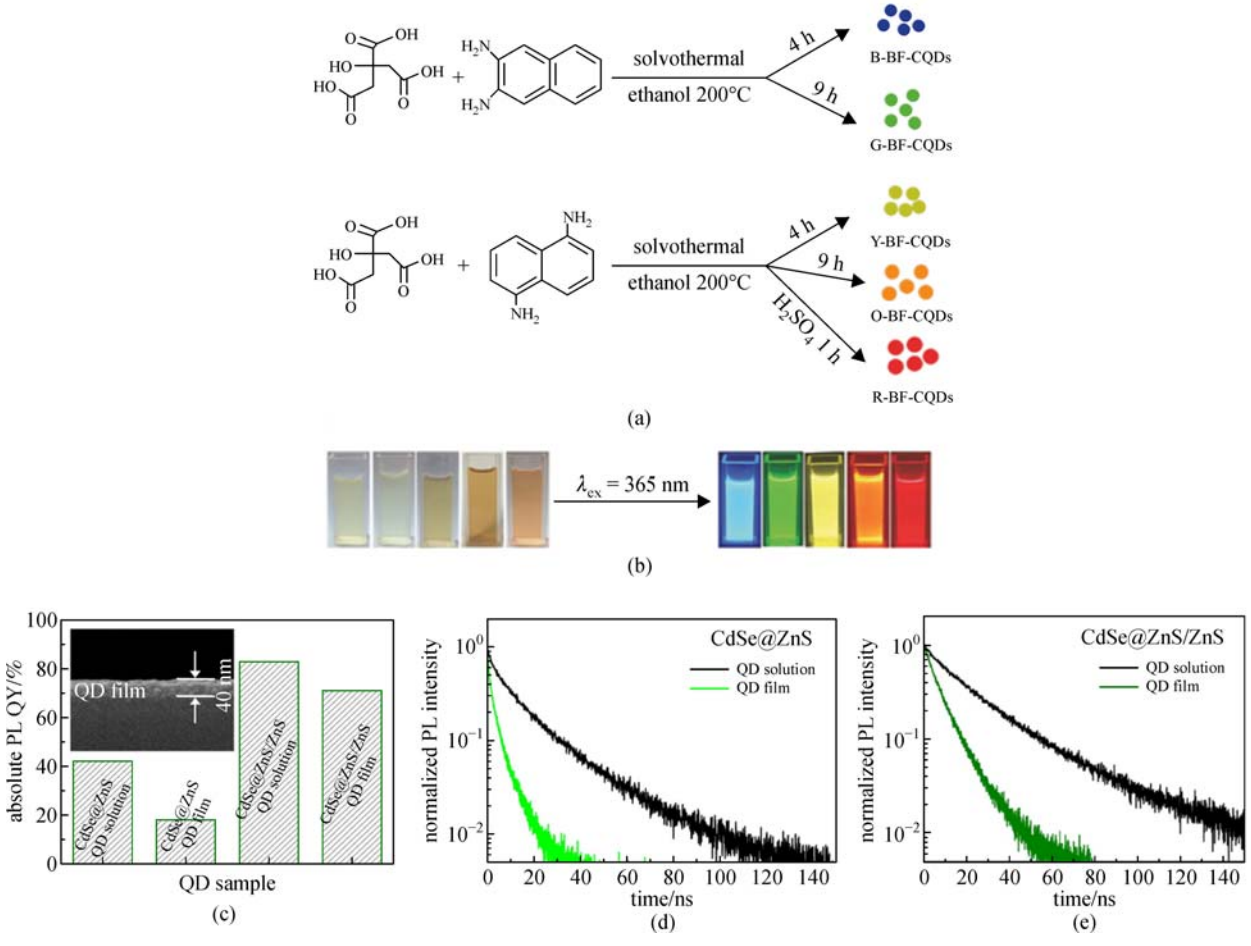

Fig. 5 (a) Synthesis mechanism of multicolor CQDs via solvothermal methods. (b) Images of multicolor CQDs with (left) and without (right) UV irradiation. Adapted with permission from Ref. [70]. Copyright 2017, John Wiley & Sons, Inc. (c) Comparison of PLQYs of CdSe/ZnS and CdSe/ZnS/ZnS QDs in solution phase versus solid film. PL decay curve in solution versus in solid film of (d) CdSe/ZnS and (e) CdSe/ZnS/ZnS QDs. Adapted with permission from Ref. [76]

QLEDs based on these alloyed QDs were up to 46.4 cd/A and 12.6%, respectively. Such excellent performance is mainly ascribed to the effective suppression of Förster energy transfer and Auger recombination in the compact QD EML. Surface ligands play an indispensable role in providing passivation to surface defect sites; however, high-density ligands insulate the QD and reduce the exciton concentration in the core. Li et al. [80] investigated the influence of the surface ligand density of perovskite QDs on the device performance. They used a hexane/ethyl acetate mixture to treat perovskite $CsPbBr_3$ QDs to balance the ability of surface passivation and charge injection. Consequently, the QLEDs exhibited a 50-fold EQE improvement to 6.27%.

Currently, cadmium-based QDs have overwhelming advantages over cadmium-free QDs in terms of optical properties and stability. For example, the highest-performance red, green, and blue QLED devices (EQE = 20.5% [81], 21% [82], and 12.2% [83], respectively) all contained cadmium-based QDs. The lifetimes of red and green devices could, respectively, reach 300000 and 90000 h [84], far exceeding the 10000 h requirement of commercial display applications. However, the lifetime of blue QDs is still two orders of magnitude shorter than that of red and green QDs, which hinders the development of full-color QLED devices.

3 Key aspects of film formation via inkjet printing

3.1 Ink printability

Highly uniform films without pinholes, coffee rings, and interfacial intermixing are indispensable for reducing the leakage current and ensuring the operation stability and durability of multilayer-stacked LEDs, whose performance substantially relies on the ink formulation with respect to the fluid properties, spreading, and drying processes. Ink formulation is essential to achieve reliable film properties as each inkjet printer has unique fluid rheological requirements for inks. In other words, the characteristics of ink, such as viscosity, surface tension, suspended particle size, and concentration, determine its printability. Generally, Z number is used to indicate the printability of ink [85,86]:

$$Z = \frac{\sqrt{\gamma \rho \alpha}}{\eta},$$

where γ, ρ, α, and η represent the surface tension, density, characteristic length (typically drop diameter), and viscosity, respectively. Moon et al. [87] demonstrated that a stable droplet was obtained in the case of $4 \leqslant Z \leqslant 14$. At a high value of Z, the corresponding low viscosity easily generates many satellite pots surrounding the main drop. Inversely, at a low value of Z, high viscosity prevents ink ejection, thus easily causing clogging in the print head. Specifically, Liu et al. [86] summarized the fluid property requirements of functional metal oxide ink for the continuous mode and DOD mode, as presented in Table 1. The viscosity and surface tension required for printing in two modes are slightly different. DOD mode has higer upper limit of viscosity and higher lower limit of surface tention requirement compared to continuous mode. For most ink systems, the viscosity depends on its solute content, which facilitates the regulation of viscosity by varying concentration. For polymer ink, the solid content is generally 0.2%–2.5% (mass fraction). The viscosity increases with the increase in solute content [88]. However, for small molecules, the solute content has a negligible contribution to the ink viscosity; thus, a high-viscosity solvent should be selected or additives should be added to improve the viscosity to satisfy the requirements of print parameters.

The volatilization rate of ink is dominated by the boiling point (B.P.) and surface tension of its solvent. During the drying process, a solvent should not evaporate too fast to prevent the precipitated solute from blocking the nozzles. By selecting a proper solvent and introducing drying agents, solvent evaporation can be precisely controlled, which in turn regulates the final patterns. For instance, a high B.P. solvent is usually added to a volatile ink system with a low B.P. in order to suppress the puzzling coffee-ring effect.

3.2 Control of coffee-ring effect

The coffee-ring effect has been a major challenge for producing uniform surface profiles with an inkjet ink composed of colloidal particles, nanoparticles, small molecules, or polymer molecules. In 1997, Deegan et al. [89] formally reported the coffee-ring effect for the first time. They argued that the coffee-ring effect was relevant to suspended spherical particles in ink. When a droplet is dropped on a substrate, the evaporation rate of its edge is faster than that of the central part, resulting in an external capillary flow in the droplet. The suspended particles are

Table 1 Fluid properties requirements of ink

mode	driver	particle size/μm	viscosity (cP)	surface tension/(dynes·cm^{-1})	density/(g·cm^{-3})
continuous		< 1	1 – 10	25 – 70	~ 1
DOD	thermal	< 1	5 – 30	35 – 70	~ 1
	piezoelectric	< 1	1 – 20	35 – 70	~ 1

Adapted with permission from Ref. [86]

carried to the droplet edge during the external flow process and precipitate, thus forming a circular ring pattern after the solvent completely evaporates. For LEDs devices, homogeneous and pinhole-free active layer films are essential to reduce the leakage current and ensure working stability. Accordingly, controlling the coffee ring via ink modification and post-treatment after deposition is crucial to realize high-precision patterns for high-performance devices.

First, reducing the outward capillary flow in droplets is an effective strategy to overcome the coffee-ring effect. In 2011, Yunker et al. [90] revealed the effect of the shape of suspended particles on the coffee ring. They used ellipsoidal suspended particles with an anisotropic shape in solution to destroy the tricky coffee-ring effect. The existence of elliptical particles caused fluctuations at their interfaces, generating strong attraction among the particles, which offset the driving power generated by the concentration difference between the edge and center of the droplet. This finding provided a new method to achieve uniform deposition of inks with solid particles. Soltman and Subramanian [91] observed that PEDOT droplets evaporated very slowly when the temperature of the substrate was reduced without considering the temperature dependence of surface tension. Thus, a balanced volatilization occurred between the droplet periphery and droplet center, which in turn slowed down the outward capillary flow and eliminated the coffee ring phenomenon.

Second, increasing the inward Marangoni flow [92] is also an effective strategy for the elimination of the coffee-ring effect. Adding additives including a high B.P. solvent and surfactant to modify the volatilization rate of the solvent and surface tension of the droplets is a simple and customary method. Kim et al. [93] used ethylene glycol (EG) with high B.P. and low surface tension to mix with Ag NPs ink. As the evaporation rate of the droplet edge of the water solvent was faster than that of the droplet center and the volatilization rate of EG was slower than that of water, the EG concentration on the edge gradually increased beyond the central concentration. Therefore, the droplet edge and droplet center generated a difference in surface tension, causing accelerated Marangoni flow. Finally, the coffee ring was eliminated owing to the accelerating Marangoni flow. Furthermore, Still et al. added an ionic surfactant, sodium dodecyl sulfate, to the droplets. The outward capillary flow brought the surfactant to the droplet periphery and formed a monolayer film at the interface between the atmosphere and ink drop. The surface tension at the droplet edge was reduced, leading to a circumfluence from the periphery to the central part. Eventually, a relatively uniform deposition film was obtained [94].

We realized coffee-ring-free green QD films on a polyetherimide (PEI)-modified ZnO layer by using varying volume ratios of 1,2-dichlorobenzene (oDCB) with cyclohexylbenzene (CHB) as the solvent. As shown in Figs. 6(a) and 6(b), when the volume ratio of oDCB was 20%, a uniform flat QD emitting pot was obtained, which was attributed to the following two key factors. On the one hand, PEI-modified ZnO demonstrated an increase in the surface energy and reduction in the contact angle. On the other hand, adding oDCB to CHB solutions reduced the surface tension. Thus, the volatilization of solvent-enabled flat printed patterns was accelerated. We further printed the QD lines by modifying the ink formulation. The printed lines demonstrated a uniform emission with a sharp edge (Figs. 6(c) and 6(d)). By scanning six points of a printed line with the length of 15 mm, we observed that they had almost the same thickness (Fig. 6(e)). Consequently, the QLEDs based on these coffee-ring-free emitting layers exhibited the peak luminance up to 12000 cd/m^2 and peak CE of 4.5 cd/A (at 1500 cd/m^2) [95].

3.3 Strategies of high-resolution pixel arrays

High-resolution display panels with ultra-fine subpixels illustrate more details of an image on the display. Two main approaches are devoted to increasing the pixel resolution: minimizing the feature size of the droplets generated by the printed head and controlling the surface properties of the substrate.

The inkjet-printed resolution highly hinges on the droplet size. The determinants of the size of the ejected droplets include the diameter of the nozzle, the electrical pulse waveform used to generate the droplets, and the physical properties such as surface tension. The original method to reduce the size of the droplets is to utilize nozzles with smaller diameters. For example, in the Dimatix D-128 inkjet-printed system, when the nozzle diameter is reduced from 21 to 9 μm, the volume of the standard ejected droplet decreases from 10 to 1 pL [96]. However, employing large batches of nozzles with a diameter of less than 9 μm would increase the clogging risk. Apart from the clogging caused by the large solid particles, there is a significant possibility of ejection failure owing to the large resisting capillary pressure [85]. In this case, considering the nozzle clogging, the viscosity, suspended particle size, surface tension, and volatilization rate of the ink all require additional optimization. However, the manufacturing cost increases imperceptibly. Another way to adjust the droplet volume is to optimize the waveform and voltage of the electric pulse that drives the ink droplets. Higher driving voltage leads to greater deformation of the piezoelectric element, thus generating a bigger droplet ejected at a faster speed. With the development of IJP technology, the driving pulse waveform also changes from the simplest unipolar waveform to a complex bipolar waveform [96]. In other words, compared with the only push force generated by the unipolar waveform, the bipolar waveform can generate both push and pull forces. This optimization separates the droplets from the ink within the cavity, and hence, the

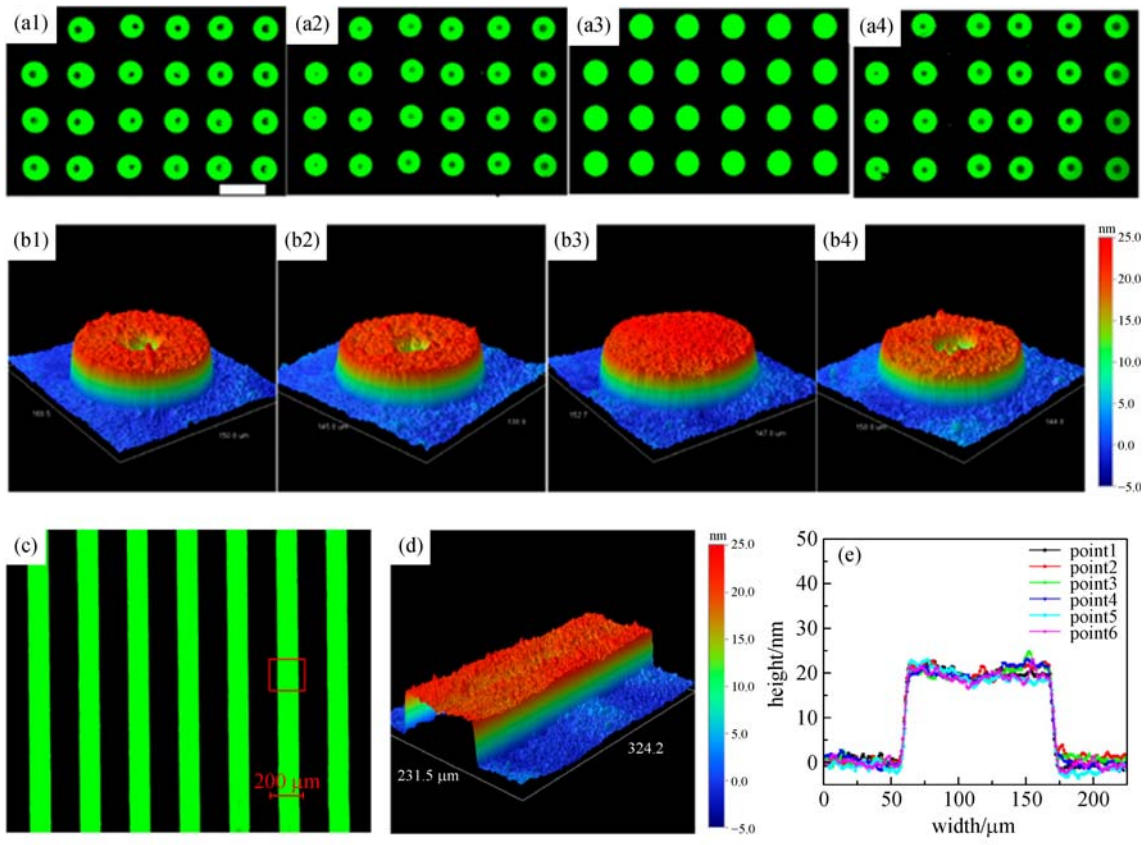

Fig. 6 (a) PL microscopic images of distributed printed dot array on PEI modified substrate (a1–a4: QD inks with volume ratios of 0, 10, 20, and 30% oDBC). (b) 3D morphology image of a1–a4 single dot; (c) PL image of printed lines; (d) 3D morphology image of printed line in (c); (e) film thickness profile of 6 points. Adapted with permission from Ref. [95]

droplet volume is reduced and the satellite is eliminated simultaneously [97–100].

The surface properties of the substrate also play a significant role in the resultant deposited pattern size. The spreading and retracting behaviors of the printed droplets are governed by the substrate wettability. Nogi et al. [101] decreased the wettability of polyimide (PI) substrate by introducing repellent pore structures based on thermally stable polyamideimide. The printed line composed of Ag NPs ink exhibited a sharp periphery without ink splashing, indicating that the treated PI structure effectively suppressed arbitrary spreading of the ink. Lam et al. [102] produced a PET (Polyethylene terephthalate) substrate with well-defined hydrophilic and hydrophobic regions by coating hydrophilic APTMS (3-aminopropyl trimethoxysilane) and hydrophobic 3M Novec 1700 and exposing to plasma or UV/O_3 with a Ni mask (Fig. 7(a)). The water contact angle (WCA) of these modified PET substrates was elastically adjustable from $< 5°$ in hydrophobic regions to approximately 105° in superhydrophilic regions (Fig. 7 (b)). In the IJP test on the selective modified PET substrate, the line width of the PEDOT: PSS was reduced to 35.5 μm, which was evidently smaller than the diameter of the inkjet droplet (approximately 55 μm) (Fig. 7(c)). This result suggested that selective wetting treatment also restricted the ink spreading and enhanced the pattern solution. In contrast to the above treatment, a substrate with a well-designed pattern named "pixel pit" forces inks to deposit precisely without any spontaneous spreading. Generally, the surfaces of the pixel pits are treated by physical or chemical methods to further facilitate printing the desirable pattern. Frisbie et al. [103] developed a series of electronic devices on special substrates with microchannels. The active ink precisely filled the channels with varying dimensions driven by capillary forces. This approach involving imprint lithography possesses immense potential to inkjet-print nanoscale patterns. Similarly, Sung et al. [104] combined IJP with transfer printing to create an innovative liquid-bridge-mediated transfer technique. The ejected ink was favorably transferred to the specified location with a nanoscale feature size.

4 OLED and QLED prototypes

Among the display equipment, OLEDs and QLEDs are emerging as promising devices for the application to multicolor EL displays, solid-state illumination, indicator

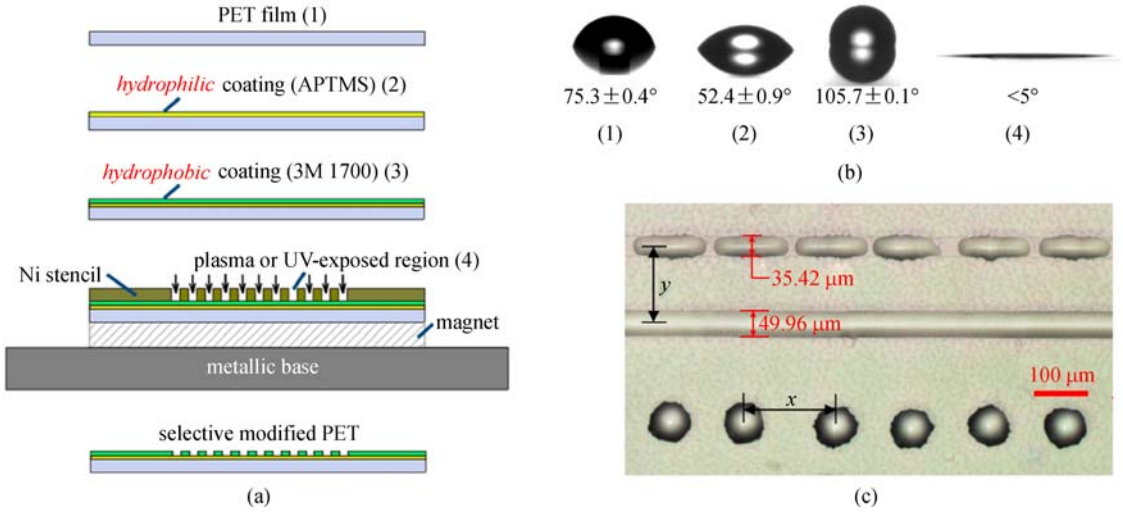

Fig. 7 (a) Preparation of patterning PET film by wetting and dewetting treatment. (b) WCA on various post-treatment PET surfaces: (1) untreated PET film, (2) treated by hydrophilic APTMS, (3) treated by hydrophobic 3M Novec 1700, (4) selectively hydrophilic treatment by either O_2/Ar plasma or UV/O_3. (c) IJP test on type b-4 PET film. Adapted with permission from Ref. [102]

lights, etc. OLEDs are further categorized into PLEDs and small-molecular organic light-emitting diodes (SMOLEDs) according to the molecule weight of the emitter. Since they were first reported by Tang and VanSlyke [3] and Friend et al. [4], respectively, intensive work on the material synthesis and architectural design, in addition to the understanding of luminescence mechanism, has resulted in remarkable improvement in the device performance and lifetime. The forward-viewing PE and EQE of white SMOLEDs fabricated via thermal vapor deposition reached 105 lm/W and approximately 30%, respectively, without any internal and external light extraction technology [105]. By contrast, the highly efficient solution-processing white tandem OLEDs showed a peak PE of 14.1 lm/W and a peak EQE of 28.0% at 5000 cd/m^2 [106]. The performance difference suggests that there is much room for performance enhancement in solution-processing OLEDs. Compared with OLEDs containing traditional organic emissive dyes, QLEDs with new types of inorganic emitters have gradually become the research focus. Owing to the significant advances in the material synthetic chemistry and the understanding of device operating mechanisms, the EQE of RGB tri-monochrome QLED devices was improved to 20.5% [81], 21% [82], and 12.2% [83].

With the FPDs favoring large area and high resolution, IJP is subject to unprecedented attention owing to the possibility of achieving these targets by replacing the expensive thermal vapor deposition method for fabricating EL devices in the foreseeable future. To inkjet-print an LED display, it is of paramount importance to ensure the film quality of each functional layer by considering multiple issues, including ink formulation modification, droplet formability, droplet size regulation, ejecting velocity, geometric precision, droplet spreading behavior, wettability of substrate, and drying process [107]. Some of the primary factors influencing the ultimate film morphology were discussed in Section 3. Combined with these key points and device physics, we will list and analyze some inkjet-printed EL devices in this section. To date, there have been numerous inkjet-printed EL devices reported by both industrial and academic communities. As presented in Table 2, we have summarized the highlights of some representative work, including active-matrix and passive-matrix OLEDs and QLEDs.

4.1 Polymer light-emitting diodes (PLEDs)

Since the earliest reported inkjet-printed PLED was demonstrated by Hebner et al. in 1998 [108], the promising film-deposited technique has been extensively employed to fabricate EL devices. In 2000, Seiko Epson [109] reported an active matrix (AM-) full-color PLED display fabricated on a polysilicon thin film transistor (PS-TFT) substrate with polyimide isolation columns, marking the first step in the application of the IJP technology to AM-PLED displays. In 2002, Philips [110] reported monochrome and full-color passive matrix (PM-) PLEDs with the sub-pixel sizes of 300 μm × 300 μm and 100 μm × 300 μm, respectively. The resolution of the full-color PM-PLED reached 64 × 96 pixels. In 2004, Philips [111] demonstrated a 2.6-inch full-color AM-PLED prototype (Fig. 8 (a)) with the resolution of 176 × 220 driven by a low-temperature polysilicon thin film transistor (LTPS-TFT) backplane. The peak luminance was enhanced to 250 cd/m^2. In 2006, Samsung and Cambridge Display Technology (CDT) [113] demonstrated a 14.1-inch full-color AM-PLED (Fig. 8(b)) driven by a-Si TFT backplane. The

Table 2 Summary of reported printed EL displays (OLEDs and QLEDs)

year	technique	printed layer	specifications	reference
1998 Hebner et al.	PLED by IJP [a]	EML (polyvinylcarbazol (PVK): coumarin 6/47 (C6/47) or nile red)	far worse than spin coating devices	[108]
2000 Seiko Epson	AM-PLED by IJP	EML (RPPV or PPV)	size: 2 inch pixel size: 11 μm × 82 μm luminance: ~ 30 cd/m^2 power consumption: ~ 0.7 W	[109]
2002 Philips	PM-PLED by IJP	HTL(PEDOT:PSS) EML(polyfluorenes(PF) and poly phenylene vinylene (PPV))	full color sub-pixel size: 100 μm × 300 μm resolution: 64 × 96	[110]
2004 Philips	AM-PLED (LTPS-TFT) by IJP	HTL (PEDOT:PSS) EML	full color size: 2.6 inch resolution: 176 × RGB × 220 sub-pixel size: 79 μm × 237 μm peak luminance: 250 cd/m^2 CIE: R (0.66, 034), G (0.39, 0.58), B (0.16, 0.22)	[111]
2004 Philips	AM-PLED (LTPS-TFT) by IJP	HTL (PEDOT:PSS) EML	full color size: 13 inch (16:9) resolution: 576 × RGB × 324 sub-pixel size: 165 μm × 501 μm peak luminance: 600 cd/m^2 frame rate: 50–60 Hz panel thickness: 1.2–2 mm	[107]
2004 Osram	PM-PLED by IJP	HTL (PEDOT:PSS) EML	full color resolution: 160 × RGB × 128 pixel size: 100 mm × 300 mm refresh rate: 74 Hz	[112]
2006 Samsung and CDT	AM-PLED (a-Si TFT) by IJP	HTL (PEDOT:PSS) EML	full color size: 14.1 inch resolution: 1280 × RGB × 768 pixel size: 80 μm NTSC (%): 53%	[113]
2006 Sharp	AM-PLED (Continuous Grain Silicon backbone) by IJP	HTL (PEDOT:PSS) IL (interlayer) EML (polyfluorenes(PF) type)	full color size: 3.6 inch (16: 9) resolution: 640 × RGB × 360 pixel size: 0.042 mm × 0.126 mm PPI: 202 luminance: 200 cd/m^2 aperture ratio 24.5%	[114]
2009 Seiko Epson	AM-PLED (LTPS-TFT) by IJP	HTL IL (interlayer) EML	size: 14 inch ppi: 60 aperture ratio: 40% color: 6-bit full color luminance: 200cd/m^2	[115]
2013 Zheng et al.	PM-PLED by IJP	Cathode (Ag NPs)	full color display area: 32.97 × 21.03 mm^2 resolution: 96 × RGB × 64 pixel size: 0.33 mm × 0.33 mm fill factor: 58% gray level: 32 × 32 × 64 = 65536	[116]
2013 AU Optronics	AM-OLED (IGZO-TFT) by IJP	HIL HTL EML	full color size: 14 inch resolution: 960 × RGB × 540 PPI: 79 luminance: 200 cd/m^2 NTSC: 74.8% aperture ratio: 24%	[117]

(*Continued*)

year	technique	printed layer	specifications	reference
2014 AU Optronics	AM-PLED (aITZO-TFT) by IJP	HIL HTL EML	full color size: 65 inch (1430 mm × 800 mm) resolution: 1920 × RGB × 1080 ppi: 34 luminance: 200 cd/m^2 NTSC: 75% aperture ratio: 30%	[118]
2017 JOLED	AM-OLED (LTPS-TFT) (the emitter type is unkown) by IJP	–	full color size: 21.6 inch resolution: 3840 × 2160 ppi: 204 luminance: 350 cd/m^2 contrast ratio: 1000000: 1 panel thickness: 1.3 mm panel weight: 500 g	[119]
2015 Olivier et al.	SMOLED by IJP	HTL (QUPD) EML (f-CHO-Acr)	display area: 0.44 cm^2 luminance: < 10 cd/m^2 CE (at 10 V): 0.008 cd/A PE (at 10 V): 0.003 lm/W	[120]
2010 Haverinen et al.	QLED by IJP	EML (RGB QDs)	full color resolution: 640 × 480 peak luminance: 350 cd/m^2 EQE = 0.24% (at 100 cd/m^2)	[121]
2011 Samsung	AM-QLED (HIZO-TFE) by transfer printing	EML (RGB QDs)	full color size: 4 inch resolution: 320 × RGB × 240 ppi: 100 aspect ratio: 4:3 brightness: 100 cd/m^2 pixel size: 46 μm × 96 μm aperture ratio: 25%	[122]
2015 Kim et al.	QLED by EJP [b]	EML (CdSe/CdZnSeS green or CdSe/CdS/ZnS red QDs)	green QLED: EQE = 2.5%, peak luminance = 36000ced/m^2 red QLED: EQE = 2.6%, peak luminance = 11250ced/m^2	[123]
2016 Han et al.	QLED by IJP	EML (CdSe/CdS/ZnCdS QDs)	turn-on voltage: 2.6 V peak brightness: 2500 cd/m^2 peak CE: 0.29 cd/A ppi: 73 pixel size: 60 μm × 180 μm	[124]
2017 Liu et al.	QLED by IJP	EML (CdSe/CdS QDs)	turn-on voltage: 1.9 V (red) pixel size: 67 μm × 170 μm ppi: 73	[125]
2017 Jiang et al.	AM-QLED (MOTFT) by IJP	ETL (ZnO NPs) EML (RGB QDs)	size: 2 inch resolution: 200 × RGB × 150 sub-pixel size: 70 μm × 210 μm ppi: 120 aperture ratio: 35%	[126]

a: inkjet printing; b: electrohydrodynamic jet printing

display panels had a high resolution of 1280 × 768 pixels and an NTSC color gamut of 53%. In the same year, Sharp [114] reported a 3.6-inch full-color AM-PLED display (Fig. 8(c)) with a high resolution up to 202 PPI. The authors inkjet-printed three active layers including PEDOT:PSS as HTL, polyfluorene type as emissive layers, and an interlayer by using 7 pl inkjet heads. The high resolution was attributed to the tiny droplets generated by the smaller printed heads, together with the optimized ink formulation and modified surface of the pixel pitches. In 2009, Seiko Epson [115] developed a new injected head that could precisely control the ejected droplet volume with an adjustable input signal. Using this improved inkjet method, a 37-inch large AM-PLED with high resolution of

up to 1920 × 1080 pixels and uniform emission driven by an LTPS-TFT backplane was developed. Furthermore, its luminance was 200 cd/m^2. In 2014, AU Optronics Corporation [118] presented a 65-inch AM-OLED panel driven by a-ITZO TFTs (Fig. 8(d)). Herein, 40 nm HIL, 30 nm HTL, and 50–110 nm EML were deposited via IJP, whereas the ETL and cathode Al were prepared via vacuum deposition. In the IJP process, the droplets were precisely dropped into the corresponding elliptical R-G-B pixel pockets without contaminating each other. By adopting a multistep drying approach under a suitable vacuum condition, they realized an extremely high degree of pixel uniformity. The corresponding specifications of this inkjet-printed prototype with unprecedented size are presented in Table 2, which satisfied the commercial requirements. Subsequently, in 2015, AU Optronics Corporation [128] demonstrated 200-PPI display panels by reshaping the bank structure with a deducted width of 34.5 μm and reducing the drop volume to 7 pL for a droplet (Fig. 8(e)). In this work, they proposed a concept called total position precision (TPP) to define the required precision for high-resolution IJP devices (Fig. 8(f)). The TPP highly depended on the machine accuracy (M), which in turn limited the resolution of the deposited pattern. At Cebit 2017, JOLED [119] demonstrated a 21.6-inch active matrix organic light-emitting diode (AMOLED) prototype based on IJP. Impressively, it exhibited outstanding characteristics with super-high resolution up to 3840 × 2160 (204 PPI), brightness of 350 cd/m^2, wide color gamut up to 130% (sRGB), and low weight of only 500 g, which were comparable to those of vacuum-evaporated panels. Furthermore, JOLED has planned to start mass producing for medical applications in the near future.

The aforementioned PLED panels could not completely eliminate the evaporated deposition technique. Typically, the EML and its adjacent charge transport layers are prepared via IJP, whereas the other functional films are formed via spin-coating or vacuum evaporation. The primary reason is that overcoming the obstacle of intermixing of multilayer films remains one of the biggest challenges in all solution-processing devices. For this scientific conundrum, several approaches have been proposed to suppress intermixing, such as the utility of orthogonal solvents [129], crosslinking reaction [130], phase separation [131], and inserting buffer layers [132]. In 2013, all solution-processed monochrome and full-color PM-PLEDs with inkjet-printed Ag-NP-based cathodes were demonstrated in our laboratory ((Figs. 9(g)–9(l)) [116]. For monochrome devices, we used poly(2-methoxy-5-(20-ethyl-hexoxy)-1,4-phenylene-vinylene) (MEH-PPV) (Fig. 9(e)), poly[2-(4-(30 ,70-dimethyloctyloxy)-phenyl)- p-phenylene-vinylene] (P-PPV) (Fig. 9(c)), and G0 (a blue emission dendrimer) (Fig. 9(f)) as the red, green and blue emitters, respectively. Similar to most reports, red and green devices exhibited a better performance than the blue device. Particularly, an additional PVK HTL was deposited on PEDOT:PSS HIL via spin coating repeatedly to enhance the performance of the GO-emitter-based blue display panel. In the fabrication process of full-color display panels, a layer of poly[3,7-dibenzothiophene-S,S-dioxide-co(9,9- dioctyl)-2,7-fluorene] (PF-FSO) (Fig. 9(a)) blue emitter was spin coated first to obtain EML with a repetitive red, green, and blue pixel array. In the subsequent process, the PFO-DHTBT (Fig. 9(d)) red emitter and the P-PPV green emitter were deposited on the corresponding pixel pits via IJP. Owing to the high-

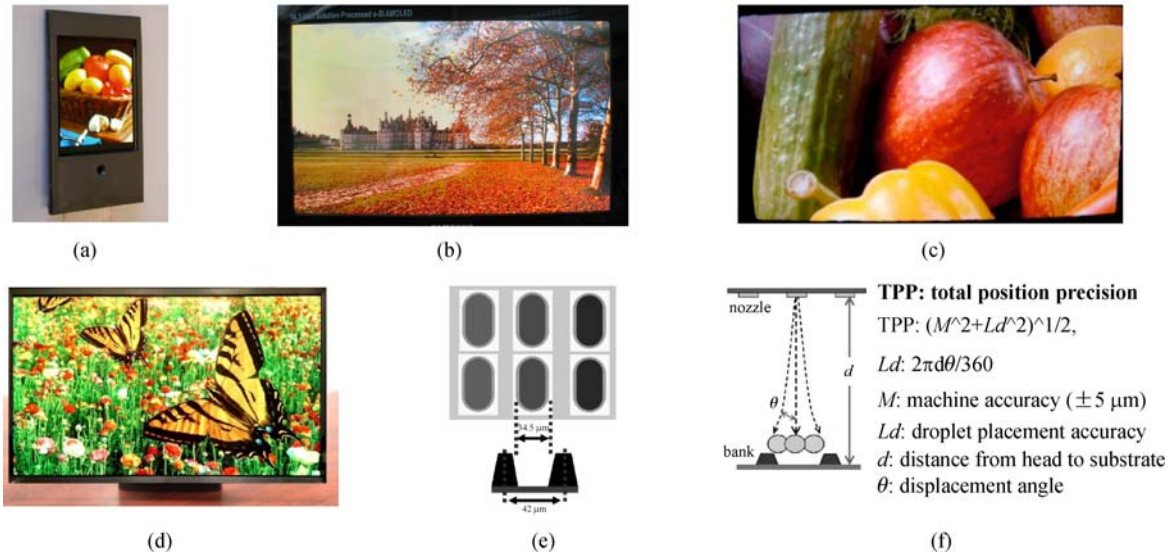

Fig. 8 (a)–(d) Light-on image of the full-color display panels fabricated by inkjet printing; (e) pixel structure for the 200-ppi device; (f) formula of TPP. Adapted with permission from Refs. [111,113,114,118,128]

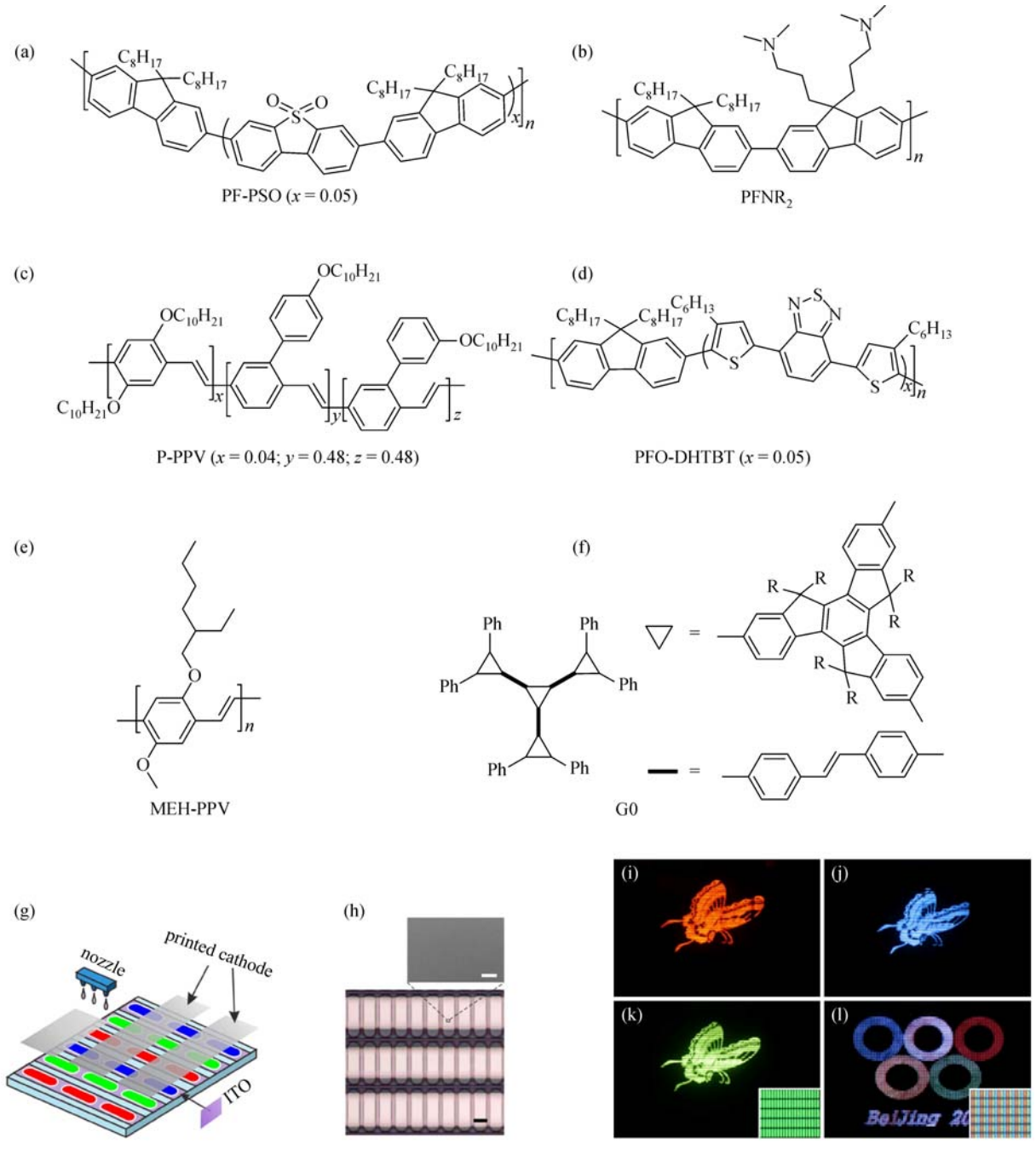

Fig. 9 (a)–(f) Chemical structures of emitters and modified molecules. (g) Schematic illustration of pixel array architecture of full-color panel. (h) Microscopic image of the backplane. PL images of (i) Red, (j) blue and (k) green monochrome displays under UV light. (l) Full-color display under UV light. Adapted with permission from Ref. [116]

efficiency energy transfer from PF-PSO to PFO-DHTBT and P-PPV, stable red and green emissions were obtained. Inkjet-printed Ag NPs was utilized to replace the traditional evaporated cathode. Before Ag NP ink deposition, we innovatively inserted a buffer layer (BL) composed of a new water/alcohol-soluble conjugated polyfluorene polyelectrolyte PFNR (poly[(9,9-bis(3′-(N, N-dimethylamino)propyl)-2,7-fluorene)-alt-2,7-(9,9-dioctyl fluorene)]) (Fig. 9(b)) synthesized by ourselves and a curable epoxy adhesive into the interface of EML and the printed Ag-NPs-based cathode. The optimized BL acted as a cross-linkable EIL for facilitating electron injection, and moreover, prevented solvent penetration from the cathode to the EML in the printing process. Ultimately, a 1.5-inch full-color PM-PLED was obtained without any defective pixels and defective lines (Fig. 9(l)). Some key parameters of the aforementioned PLED panels are given in Table 2.

4.2 Small-molecular organic light-emitting diodes (SMOLEDs)

In contrast to polymers with an inherent solution-processing nature, small molecules are generally deposited via high-vacuum vapor deposition. Despite the immense success of the commercialization of SMOLEDs in mobile-phone and television displays, the mass production scale-up is still constrained by the sophisticated apparatus and high cost. Nevertheless, owing to the facile molecular design and outstanding performance of thermal vacuum-deposited devices, many groups have attempted to fabricate SMOLEDs using solution processing, especially the promising IJP technology.

Yang et al. [133] reported R-G-B multicolor OLEDs with hybrid EMLs via IJP. Herein, PVK acted as the blue EML and served as the host material for red and green EMLs, whereas $Almq_3$ (tris(4-methyl-8-quinolinolato)Al (III)) and DCM (4-(dicyanomethylene)-2-methyl-6-(4-dimethylaminostyryl)-4H-pyran) were used as the dopants. Although the device efficiency of the inkjet-printed OLED was approximately 10 times lower than those fabricated using the thermal sublimation process, it opened an avenue to deposit small molecules using a solution process. Gorter et al. [134] utilized the IJP technique to deposit HIL (PEDOT:PSS), HTL (α-NPD), and EML (Alq_3) of SMOLEDs. In comparison with these vacuum-deposited devices, the printed devices exhibited poor efficiency and nonuniform brightness. They attributed such inferior performance to the redissolution and crystallization of α-NPD when IJP Alq_3. Therefore, interfacial intermixing is an enormous challenge to be solved urgently. In order to avoid intermixing, Olivier et al. [120] inkjet-printed QUPD (Fig. 10(a)) as HTL, and f-CHO-Acr as EML (Fig. 10(b)), followed by ultraviolet radiation and baking to photo-polymerize the small molecule. Unfortunately, the CE of the device was only 0.008 cd/A at 10 V, which was three orders of magnitude less than that of the device fabricated via the thermal evaporation technique. Furthermore, many visible dead dots and lines appeared on the surface of the operating devices. Such inferior performance was primarily due to the utility of the non-well-optimized materials. Ma et al. [135] reported SMOLEDs with an inkjet-printed EML of TBADN (2-(t-butyl)-9,10-bis (20-naphthyl) anthracene) (Fig. 10(c)) doped with DPAVBi (4,4′-bis[2-{4-(N,N-diphenylamino)phenyl vinyl]) (Fig. 10(d)). Cyclohexylbenzene or a-chloronaphthalene with high B. P. and high viscosity were added to the main solvent chlorobenzene (CB). The modified ink suppressed the dewetting behavior of pristine TBADN/ DPAVBi solutions, thus obtaining uniform EML with a proper thickness. The SMOLED based on this printed EML revealed a turn-

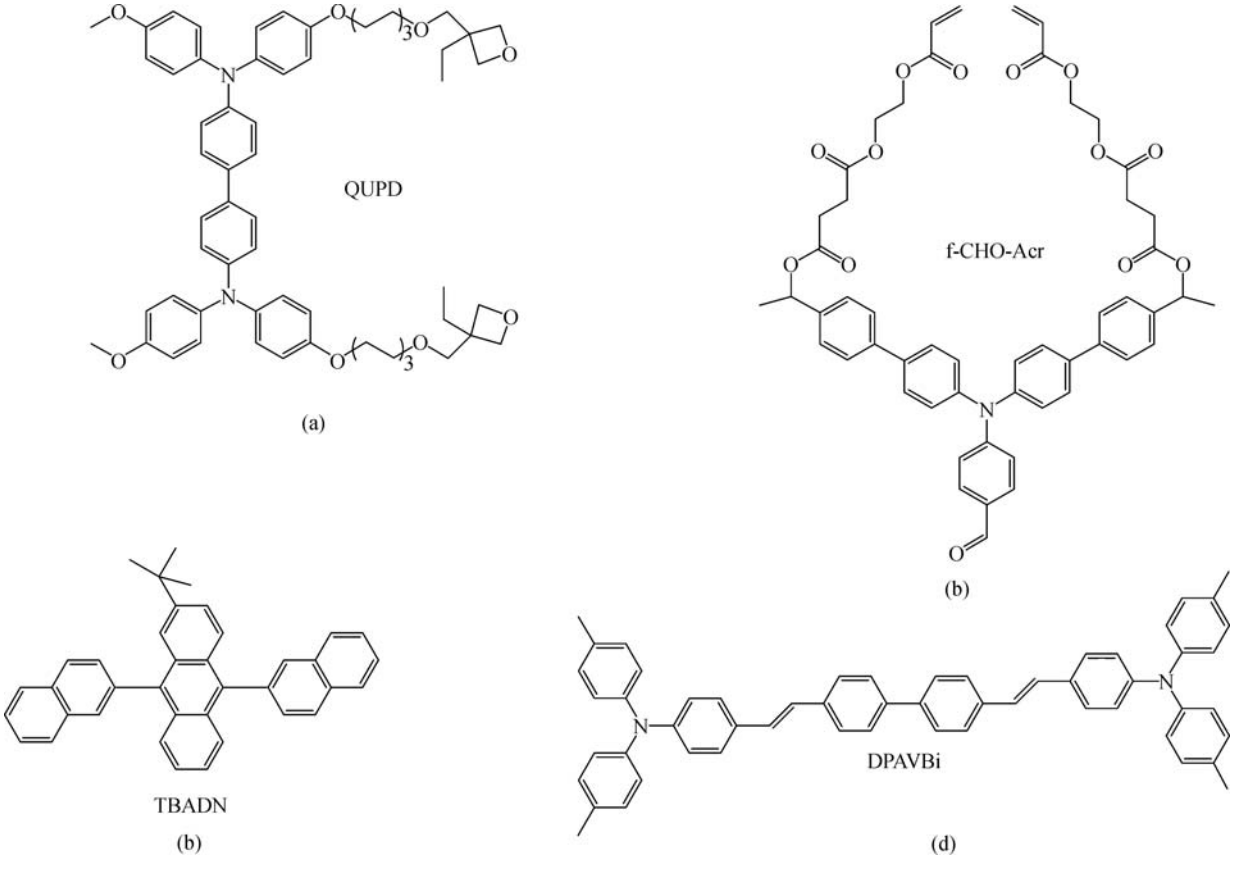

Fig. 10 Chemical structures of emitters of small molecules [120,135]. (a) QUPD; (b) f-CHO-Acr; (c) TBADN; (d) DPAVBi

on voltage of 5.5 V, peak luminance of 289 cd/m^2, and peak CE of 0.71 cd/A. Similarly, Park et al. used 5 wt.% DPAVBi-doped TVADN as rgw small-molecule emissive material, *ortho*-dichlorobenzene as the solvent to prepare ink at a ratio of 1:20 wt.%. The peak brightness, CE, and EQE of the corresponding SMOLED fabricated via electrohydrodynamic jet (e-jet) printing were optimized to 17000 cd/m^2, 8.7 cd/m^2, and 4.6%, respectively.

Seiko Epson [127] reported a series of full-color printable phosphorescent SMOLEDs with extremely high efficiency, pure emission, and long lifetime (Table 3) using spin coating, suggesting that the high-performance SMOLEDs were potentially demonstrated by IJP with a similar ink formulation. However, the inkjet-printed devices demonstrated less stability compared to those fabricated via spin coating. In summary, phase separation and crystallization in the host and dopant system are the main hindrances for obtaining uniform printing patterns. The stable emission and long lifetime depend on the surface profiles of the films. Therefore, further efforts should be made to exploit the amorphous materials with high T_g.

4.3 Quantum dot light-emitting diodes

Colloidal QDs exhibit many intriguing optical properties and intrinsic compatibility with solution processing, which render them potential substitutes for organic emissive materials. Owing to the structural similarity between QLEDs and PLEDs, their manufacturing processes are highly compatible; thus, the development of QLEDs could benefit from the relatively mature processing conditions of PLEDs.

Charge injection balance is of immense importance in device efficiency and lifetime. The first QLEDs were demonstrated by Colvin et al. [5] in 1994. In these devices, a layer of CdSe QDs as EML and a layer of PPV as HTL were directly sandwiched between two electrodes. The devices exhibited unstable emission largely owing to the unbalanced carrier injection. In 2002, Coe et al. [136] utilized TPD as HTL and TAZ and Alq_3 as ETLs to balance the charge injection and confined excitons within the monolayer of CdSe/ZnS QDs. The CE increased significantly by 1.6 cd/A. However, the hole mobility of HTLs is generally bigger than the electron mobility of ETLs for small-molecular charge transport layers. Another issue is that small molecules are prone to crystallization. These unfavorable properties reduce the device stability. Therefore, multiple inorganic metal oxide nanocrystals have been exploited to act as the charge transport layer, including n-type species (ZnO, TiO_2, SnO_2, VO_x, WO_x, and MoO_x) and p-type species (NiO) [22]. For instance, using ZnO as ETL can compensate the deficiency of the low electron mobility of small-molecular ETLs. The most efficient red, green, and blue QLEDs reported up to date all contained ZnO ETLs without exception [81–83]. Inversely, the electron mobility of ZnO is 1–3 orders of magnitude larger than the hole mobility of the organic HTL, such as PVK, Poly-TPD, and TFB. In order to balance the carrier recombination, several strategies such as inserting a thin dielectric film between ZnO and QDs [81], passivating ZnO with organic materials [137,138], and adding additives to the QD solution [139] were employed. In 2014, Peng et al. [81] reported the most efficient red-QLEDs with EQE up to 20.5%. In these devices, ZnO NPs with high electron mobility were used as ETL, Poly-TPD with high hole mobility and PVK with deep HOMO (highest occupied molecular orbital) level were used as double HTLs. In order to further balance the charge injection, a 6-nm insulating PMMA (poly(methylmethacrylate)) layer was deposited on CdSe/CdS QDs EML before spin coating ZnO ETL for blocking the redundant electrons from ZnO ETL to the QD layer.

Owing to the encouraging breakthrough in synthesizing the chemistry of QDs and the rapid growth of the efficiency of spin-coating devices, many groups have attempted to utilize various patterning methods to fabricate large and high-definition QLED prototype devices in recent years, such as transfer printing [122,140–142], electrohydrodynamic jet (e-jet) printing [123], photolithography [143–145], and IJP [95,121,126,146]. In 2011, Samsung [122] demonstrated a 4-inch full-color AM-QLEDs display driven by HIZO (hafnium-indium-zinc oxide) TFT backplane. As shown in Fig. 11(a), this display prototype had an almost perfect image owing to the high-quality QD films produced by transfer printing. In 2015, Choi et al. [142] demonstrated wearable red, green, and blue QLED arrays via high-resolution intaglio transfer printing. The feature size of each pixel could be reduced to 6 μm without obvious pixel breakage regardless of the transferring patterns, which contributed to ultrafine pixel arrays with uniform morphology and high resolution up to 2460 PPI (Fig. 11(b)). The white flexible QLED devices based on this transferring technique exhibited high luminance up to

Table 3 Performances of red, green, and blue printable phosphorescent OLEDs

device	CE/(cd·A^{-1})	CIE	lifetime/h
red at 500 cd/m^2	9	(0.66, 0.33)	53000
green at 1000 cd/m^2	35	(0.33, 0.63)	52000
light blue at 500 cd/m^2	18	(0.19, 0.40)	3000
blue at 500 cd/m^2	6	(0.15, 0.23)	1000

Adapted with permission from Ref. [127]

14000 cd/m^2 (at 7 V) and peak EQE of 2.35% (at 4.5 V). Moreover, the lifetime of the devices could reach 12815 h when subjected to the stretching test (at the initial brightness of 100 cd/m^2). However, the transfer printing technique typically required a 2–3-step deposition procedure: (a) deposit QD layer onto stamp via spin coating, (b) transfer QD layers to the receiver substrate. In this process, the manufacturing cost increases owing to the sophisticated stamp fabrication and the increased material loss.

Therefore, the advantages in the pixelating of IJP have become increasingly prominent. In 2009, Haverinen et al. [146] demonstrated the fabrication of monochromatic QLEDs via IJP. They observed that the surface profiles of QD layers depended on both the uniformity of the underlying Poly-TPD layer and the feature size of QDs. Subsequently, in 2010, Haverinen et al. [121] reported the first full-color RGB QLED devices with a resolution of QVGA (quarter video graphics array, 640 × 480) obtained via IJP. In this process, a photolithographic method was used to obtain the QVGA pixel pockets. However, the full-color devices exhibited poor performance with the peak EQE of 0.14% at 17.5 V owing to the formation of pinholes. In 2016, Han et al. [124] used IJP to produce red QD pixels, which showed uniform surface profiles with each pixel size of 60 μm × 180 μm (Fig. 11(c)). The printed red QLED devices had a peak brightness of 2500 cd/m^2 and a resolution of 73 PPI (corresponding to 60-inch 4K UHD format). Liu et al. [125] also achieved a high-quality inkjet-printed QD layer by regulating the rheological properties of the ink. Recently, we successfully fabricated 2-inch full-color inkjet-printed AM-QLEDs driven by the metal oxide thin film transistor (MOTFT) backplane (Figs. 11(d)–11(f)) [126]. The prototype with 120 PPI exhibited a peak luminance of 400 cd/m^2 and pure emission with the NTSC color gamut up to 109%. We also fabricated R, G, B monochrome PM-QLEDs via IJP to evaluate their performances. The three RGB tri-monochrome devices exhibited the peak CEs of 2.5, 13.9, and 0.3 cd/A, respectively, rendering them one of the most efficient printed PM-QLEDs devices to date. With regard to the individual sub-pixels, they exhibited uniform profiles and sharp edges without cross-contamination owing to the delicate optimization of ink formation and the hydrophilic-hydrophobic treatment of pixel-defined layers.

5 Conclusion and outlook

In this review, the technological highlights of printable emissive materials, key points for the film formation via inkjet printing, and some representative printed OLED and QLED display panels were summarized. Three kinds of emissive materials — polymer emitters, small-molecular phosphors, and colloidal quantum dots — were introduced synoptically. Their outstanding EL performances in LEDs

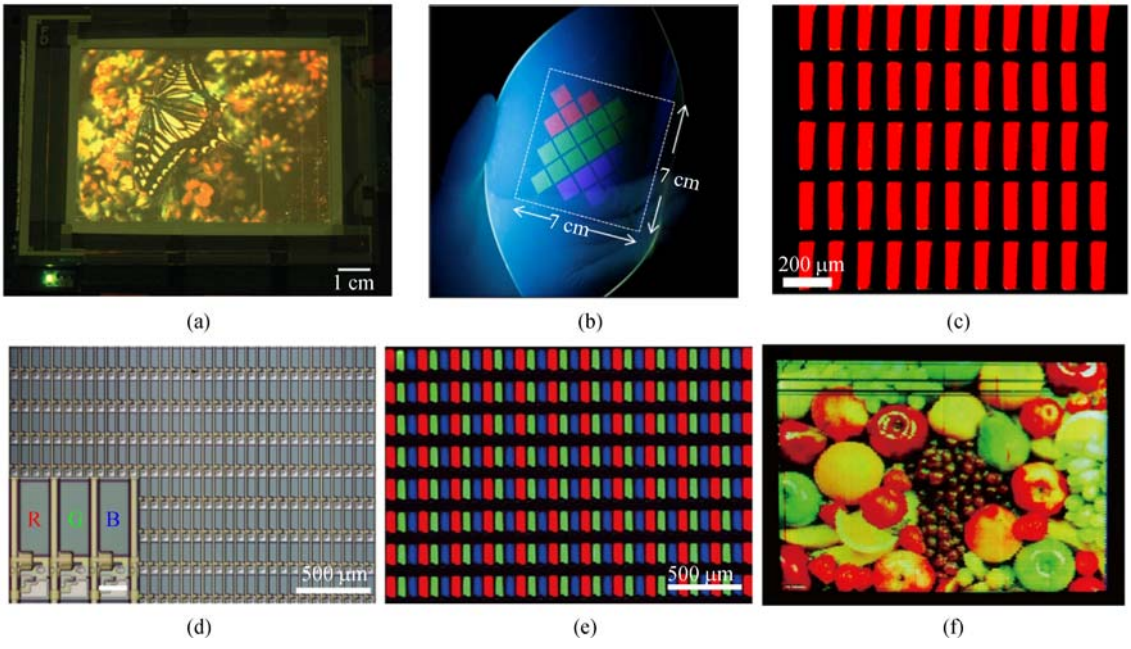

Fig. 11 (a) EL image of a 4-inch full-color AM-QLED display. Adapted with permission from Ref. [122]. Copyright © 2011, Macmillan Publishers Limited. (b) PL image of a QD dot array patterned by repeated aligned intaglio transfer printing on a PET substrate. Adapted with permission from Ref. [142]. Copyright © 2011, Macmillan Publishers Limited. (c) EL microscope image of an inkjet-printed red QLED. Adapted with permission from Ref. [124]. Copyright © 2016, John Wiley & Sons, Inc. (d) Microscopic image of pixel arrays. (Inset: enlarged image of RGB sub-pixels). (e) EL microscopic image of RGB sub-pixel arrays. (f) Photograph of 2-inch full-color AM-QLEDs display. Adapted with permission from Ref. [126]

were demonstrated via solution processing. The performances of OLEDs and QLEDs highly rely on the film quality, which is dominated by multiple impacts, such as the inkjet printer (nozzle size, control program), rheological behavior of inks (viscosity, surface tension, volatility rate), and substrate surface (surface energy, wettability, morphology). The coffee-ring effect is a common issue encountered in printing processes. Reducing outward capillary flow and accelerating inward Marangoni flow are effective coping strategies of this problem. High-resolution pixel arrays are obtained by modifying the ink formulation, reducing the nozzle diameter, optimizing the driving parameters for generating droplets, or modifying the wettability of the substrates. With the rapid development of innovative materials and device structures, substantial progress has been made in EL devices (OLEDs and QLEDs) via inkjet printing over the past two decades.

Inkjet printing is a promising technique owing to its unique advantages over the thermal-evaporated technique. First, inkjet printing is a cost-effective method. Compared to the thermal-evaporated technique, inkjet printing can reduce material consumption by approximately 90%, and it requires a low cost for equipment maintenance. Second, fine metal masks (FMM) are indispensable when manufacturing RGB tricolor SMOLEDs. However, with the increase in resolution, the mesh size of the FMM shrinks and the color mixing problem becomes difficult to control. Furthermore, it results in a substantial reduction in yield. Third, the flat panel display industry favors large size. The evaporation process will encounter an upgrading problem among Gen8 lines. By contrast, IJP is expected to realize roll-to-roll printing; thus, it is more suitable for fabricating large and flexible panels.

However, inkjet printing also faces many challenges. The biggest bottleneck is the elimination of the differential between each tiny printed point, which is vital to obtaining efficient and reliable devices. Another issue is to develop equipment for printing in ultrafine sub-pixel units, which is of immense importance to small and medium size display panels with high-density pixels. Furthermore, the existing printable ink systems are mostly inefficient and insufficiently stable, especially for blue emitters. Paradoxically, there are very few material manufacturers capable of manufacturing printable materials for OLEDs and QLEDs. Further investigation should be conducted to realize the commercialization of inkjet printing displays.

In short, opportunities and challenges exist simultaneously. In view of the encouraging recent progress and versatile nature of inkjet printing, we anticipate a promising future for this technology in the fabrication of large and high-resolution FPDs in a cost-effective way.

Acknowledgements This work was supported by the National Key Basic Research and Development Program of China (Nos. 2015CB655004, 2016YFB0401005, and 2016YFF0203603), the National Natural Science Foundation of China (Grant Nos. 21673082, U1601651, and U1301243), Guangdong Science and Technology Plan (No. 2017B090901055), the Pearl River S&T Nova Program of Guangzhou (Nos. 201710010066, and 201610010052), the Fundamental Research Funds for the Central Universities (Nos. 2017MS008 and 2017ZD001), China Postdoctoral Science Foundation (No. 2017T100627) and the Tiptop Scientific and Technical Innovative Youth Talents of Guangdong Special Support Program (Nos. 2015TQ01C777, and 2016TQ03C331).

References

1. Blasse G, Bril A. A new phosphor for flying-spot cathode-ray tubes for color television: yellow-emitting $Y_3Al_5O_{12}$–Ce^{3+}. Applied Physics Letters, 1967, 11(2): 53–55
2. Brody T P, Asars J A, Dixon G D A. 6 × 6 inch 20 lines-per-inch liquid-crystal display panel. IEEE Transactions on Electron Devices, 1973, 20(11): 995–1001
3. Tang C W, VanSlyke S A. Organic electroluminescent diodes. Applied Physics Letters, 1987, 51(12): 913–915
4. Burroughes J H, Bradley D D C, Brown A R, Marks R N, Mackay K, Friend R H, Burns P L, Holmes A B. Light-emitting diodes based on conjugated polymers. Nature, 1990, 347(6293): 539–541
5. Colvin V L, Schlamp M C, Alivisatos A P. Light-emitting-diodes made from cadmium selenide nanocrystals and a semiconducting polymer. Nature, 1994, 370(6488): 354–357
6. Baldo M A, O'brien D F, You Y, Shoustikov A, Sibley S, Thompson M E, Forrest S R. Highly efficient phosphorescent emission from organic electroluminescent devices. Nature, 1998, 395(6698): 151–154
7. Uoyama H, Goushi K, Shizu K, Nomura H, Adachi C. Highly efficient organic light-emitting diodes from delayed fluorescence. Nature, 2012, 492(7428): 234–238
8. Gather M C, Köhnen A, Meerholz K. White organic light-emitting diodes. Advanced Materials, 2011, 23(2): 233–248
9. Granlund T, Nyberg T, Roman L S, Svensson M, Inganäs O. Patterning of polymer light-emitting diodes with soft lithography. Advanced Materials, 2000, 12(4): 269–273
10. Gather M C, Köhnen A, Falcou A, Becker H, Meerholz K. Solution-processed full-color polymer organic light-emitting diode displays fabricated by direct photolithography. Advanced Functional Materials, 2007, 17(2): 191–200
11. Malinowski P E, Ke T H, Nakamura A, Chang T Y, Gokhale P, Steudel S, Janssen D, Kamochi Y, Koyama I, Iwai Y, Heremans P. 16.3: true-color 640 ppi OLED arrays patterned by CA i-line photolithography. SID Symposium Digest of Technical Papers, 2015, 46(1): 215–218
12. Jin H, Sturm J C. 40.2: super-high resolution transfer printing for full-color OLED display patterning. Sid Symposium Digest of Technical Papers, 2009, 40(1): 597–599
13. Calvert P. Inkjet printing for materials and devices. Chemistry of Materials, 2001, 13(10): 3299–3305
14. Tekin E, Smith P J, Schubert U S. Inkjet printing as a deposition and patterning tool for polymers and inorganic particles. Soft Matter, 2008, 4(4): 703–713
15. Singh M, Haverinen H M, Dhagat P, Jabbour G E. Inkjet printing-process and its applications. Advanced Materials, 2010, 22(6): 673–685

16. Zhan Z, An J, Wei Y, Tran V T, Du H. Inkjet-printed optoelectronics. Nanoscale, 2017, 9(3): 965–993
17. Cummins G, Desmulliez M P Y. Inkjet printing of conductive materials: a review. Circuit World, 2012, 38(4): 193–213
18. Kamyshny A, Magdassi S. Conductive nanomaterials for printed electronics. Small, 2014, 10(17): 3515–3535
19. Huang F, Cheng Y J, Zhang Y, Liu M S, Jen A K Y. Crosslinkable hole-transporting materials for solution processed polymer light-emitting diodes. Journal of Materials Chemistry, 2008, 18(38): 4495–4509
20. Huang F, Wu H, Cao Y. Water/alcohol soluble conjugated polymers as highly efficient electron transporting/injection layer in optoelectronic devices. Chemical Society Reviews, 2010, 39(7): 2500–2521
21. Meyer J, Hamwi S, Kröger M, Kowalsky W, Riedl T, Kahn A. Transition metal oxides for organic electronics: energetics, device physics and applications. Advanced Materials, 2012, 24(40): 5408–5427
22. Liang X, Bai S, Wang X, Dai X, Gao F, Sun B, Ning Z, Ye Z, Jin Y. Colloidal metal oxide nanocrystals as charge transporting layers for solution-processed light-emitting diodes and solar cells. Chemical Society Reviews, 2017, 46(6): 1730–1759
23. Lee Y Z, Chen X, Chen S A, Wei P K, Fann W S. Soluble electroluminescent poly(phenylene vinylene)s with balanced electron- and hole injections. Journal of the American Chemical Society, 2001, 123(10): 2296–2307
24. Saikia G, Singh R, Sarmah P J, Akhtar M W, Sinha J, Katiyar M, Iyer P K. Synthesis and characterization of soluble poly (p-phenylene) derivatives for PLED applications. Macromolecular Chemistry and Physics, 2009, 210(24): 2153–2159
25. Ding A L, Pei J, Lai Y H, Huang W. Phenylene-functionalized polythiophene derivatives for light-emitting diodes: their synthesis, characterization and properties. Journal of Materials Chemistry, 2001, 11(12): 3082–3086
26. Lee J, Cho H J, Cho N S, Hwang D H, Kang J M, Lim E, Lee J I, Shim H K. Enhanced efficiency of polyfluorene derivatives: organic-inorganic hybrid polymer light-emitting diodes. Journal of Polymer Science Part A, Polymer Chemistry, 2006, 44(9): 2943–2954
27. Wang R, Wang W Z, Yang G Z, Liu T, Yu J, Jiang Y. Synthesis and characterization of highly stable blue-light-emitting hyperbranched conjugated polymers. Journal of Polymer Science Part A, Polymer Chemistry, 2008, 46(3): 790–802
28. Hou Q, Xu Y, Yang W, Yuan M, Peng J, Cao Y. Novel red-emitting fluorene-based copolymers. Journal of Materials Chemistry, 2002, 12(10): 2887–2892
29. Guan R, Xu Y, Ying L, Yang W, Wu H, Chen Q, Cao Y. Novel green-light-emitting hyperbranched polymers with iridium complex as core and 3, 6-carbazole-co-2, 6-pyridine unit as branch. Journal of Materials Chemistry, 2009, 19(4): 531–537
30. Liang J, Zhao S, Jiang X F, Guo T, Yip H L, Ying L, Huang F, Yang W, Cao Y. White polymer light-emitting diodes based on exciplex electroluminescence from polymer blends and a single polymer. ACS Applied Materials & Interfaces, 2016, 8(9): 6164–6173
31. Liang J, Zhong Z, Li S, Jiang X F, Ying L, Yang W, Peng J, Cao Y. Efficient white polymer light-emitting diodes from single polymer exciplex electroluminescence. Journal of Materials Chemistry C, Materials for Optical and Electronic Devices, 2017, 5(9): 2397–2403
32. Liu F, Tang C, Chen Q Q, Li S Z, Wu H B, Xie L H, Peng B, Wei W, Cao Y, Huang W. Pyrene functioned diarylfluorenes as efficient solution processable light emitting molecular glass. Organic Electronics, 2009, 10(2): 256–265
33. Li Y, Li A Y, Li B X, Huang J, Zhao L, Wang B Z, Li J W, Zhu X H, Peng J, Cao Y, Ma D G, Roncali J. Asymmetrically 4,7-disubstituted benzothiadiazoles as efficient non-doped solution-processable green fluorescent emitters. Organic Letters, 2009, 11 (22): 5318–5321
34. Fan Z, Cheng C, Yu S, Ye K, Sheng R, Xia D, Ma C, Wang X, Chang Y, Du G. Red and near-infrared electroluminescence from organic light-emitting devices based on a soluble substituted metal-free phthalocyanine. Optical Materials, 2009, 31(6): 889–894
35. Inaoka S, Roitman D B, Advincula R C. Cross-linked polyfluorene polymer precursors: electrodeposition, PLED device characterization, and two-site co-deposition with poly (vinylcarbazole). Chemistry of Materials, 2005, 17(26): 6781–6789
36. Gong X, Ostrowski J C, Bazan G C, Moses D, Heeger A J. Red electrophosphorescence from polymer doped with iridium complex. Applied Physics Letters, 2002, 81(20): 3711–3713
37. Gong X, Ostrowski J C, Moses D, Bazan G C, Heeger A J. Electrophosphorescence from a polymer guest–host system with an iridium complex as guest: Förster energy transfer and charge trapping. Advanced Functional Materials, 2003, 13(6): 439–444
38. Sirringhaus H, Kawase T, Friend R H, Shimoda T, Inbasekaran M, Wu W, Woo E P. High-resolution inkjet printing of all-polymer transistor circuits. Science, 2000, 290(5499): 2123–2126
39. Liu J, Zou J, Yang W, Wu H, Li C, Zhang B, Peng J, Cao Y. Highly efficient and spectrally stable blue-light-emitting polyfluorenes containing a dibenzothiophene-S, S-dioxide unit. Chemistry of Materials, 2008, 20(13): 4499–4506
40. Li Y, Wu H, Zou J, Ying L, Yang W, Cao Y. Enhancement of spectral stability and efficiency on blue light-emitters via introducing dibenzothiophene-S, S-dioxide isomers into polyfluorene backbone. Organic Electronics, 2009, 10(5): 901–909
41. Liu J, Hu S, Zhao W, Zou Q, Luo W, Yang W, Peng J, Cao Y. Novel spectrally stable saturated blue-light-emitting poly[(fluorene)-co-(dioctyldibenzothiophene-S,S-dioxide)]s. Macromolecular Rapid Communications, 2010, 31(5): 496–501
42. Zhao L, Zou J, Huang J, Li C, Zhang Y, Sun C, Zhu X, Peng J, Cao Y, Roncali J. Asymmetrically 9, 10-disubstituted anthracenes as soluble and stable blue electroluminescent molecular glasses. Organic Electronics, 2008, 9(5): 649–655
43. Klimov V I. Mechanisms for photogeneration and recombination of multiexcitons in semiconductor nanocrystals: implications for lasing and solar energy conversion. Journal of Physical Chemistry B, 2006, 110(34): 16827–16845
44. Bawendi M G, Steigerwald M L, Brus L E. The quantum mechanics of larger semiconductor clusters (“quantum dots”). Annual Review of Physical Chemistry, 1990, 41(1): 477–496

45. Alivisatos A P, Harris A L, Levinos N J, Steigerwald M L, Brus L E. Electronic states of semiconductor clusters: homogeneous and inhomogeneous broadening of the optical spectrum. Journal of Chemical Physics, 1988, 89(7): 4001–4011
46. Wang Y, Suna A, McHugh J, Hilinski E F, Lucas P A, Johnson R D. Optical transient bleaching of quantum-confined CdS clusters: the effects of surface-trapped electron-hole pairs. Journal of Chemical Physics, 1990, 92(11): 6927–6939
47. Chan W C W, Nie S. Quantum dot bioconjugates for ultrasensitive nonisotopic detection. Science, 1998, 281(5385): 2016–2018
48. Zhang F, He X W, Li W Y, Zhang Y K. One-pot aqueous synthesis of composition-tunable near-infrared emitting Cu-doped CdS quantum dots as fluorescence imaging probes in living cells. Journal of Materials Chemistry, 2012, 22(41): 22250–22257
49. Jiang C, Liu H, Liu B, Zhong Z, Zou J, Wang J, Wang L, Peng J, Cao Y. Improved performance of inverted quantum dots light emitting devices by introducing double hole transport layers. Organic Electronics, 2016, 31: 82–89
50. Rogach A L, Gaponik N, Lupton J M, Bertoni C, Gallardo D E, Dunn S, Pira N L, Paderi M, Repetto P, Romanov S G, O'Dwyer C, Torres C M S, Eychmuller A. Light-emitting diodes with semiconductor nanocrystals. Angewandte Chemie International Edition, 2008, 47(35): 6538–6549
51. Mueller A H, Petruska M A, Achermann M, Werder D J, Akhadov E A, Koleske D D, Hoffbauer M A, Klimov V I. Multicolor light-emitting diodes based on semiconductor nanocrystals encapsulated in GaN charge injection layers. Nano Letters, 2005, 5(6): 1039–1044
52. Pattantyus-Abraham A G, Kramer I J, Barkhouse A R, Wang X, Konstantatos G, Debnath R, Levina L, Raabe I, Nazeeruddin M K, Grätzel M, Sargent E H. Depleted-heterojunction colloidal quantum dot solar cells. ACS Nano, 2010, 4(6): 3374–3380
53. Konstantatos G, Howard I, Fischer A, Hoogland S, Clifford J, Klem E, Levina L, Sargent E H. Ultrasensitive solution-cast quantum dot photodetectors. Nature, 2006, 442(7099): 180–183
54. Koh W K, Saudari S R, Fafarman A T, Kagan C R, Murray C B. Thiocyanate-capped PbS nanocubes: ambipolar transport enables quantum dot based circuits on a flexible substrate. Nano Letters, 2011, 11(11): 4764–4767
55. Nan W, Niu Y, Qin H, Cui F, Yang Y, Lai R, Lin W, Peng X. Crystal structure control of zinc-blende CdSe/CdS core/shell nanocrystals: synthesis and structure-dependent optical properties. Journal of the American Chemical Society, 2012, 134(48): 19685–19693
56. Qin H, Niu Y, Meng R, Lin X, Lai R, Fang W, Peng X. Single-dot spectroscopy of zinc-blende CdSe/CdS core/shell nanocrystals: nonblinking and correlation with ensemble measurements. Journal of the American Chemical Society, 2014, 136(1): 179–187
57. Tan Z K, Moghaddam R S, Lai M L, Docampo P, Higler R, Deschler F, Price M, Sadhanala A, Pazos L M, Credgington D, Hanusch F, Bein T, Snaith H J, Friend R H. Bright light-emitting diodes based on organometal halide perovskite. Nature Nanotechnology, 2014, 9(9): 687–692
58. Wang J, Wang N, Jin Y, Si J, Tan Z K, Du H, Cheng L, Dai X, Bai S, He H, Ye Z, Lai M L, Friend R H, Huang W. Interfacial control toward efficient and low-voltage perovskite light-emitting diodes. Advanced Materials, 2015, 27(14): 2311–2316
59. Li G, Rivarola F W R, Davis N J L K, Bai S, Jellicoe T C, de la Peña F, Hou S, Ducati C, Gao F, Friend R H, Greenham N C, Tan Z K. Highly efficient perovskite nanocrystal light-emitting diodes enabled by a universal crosslinking method. Advanced Materials, 2016, 28(18): 3528–3534
60. Wang N, Cheng L, Ge R, Zhang S, Miao Y, Zou W, Yi C, Sun Y, Cao Y, Yang R, Wei Y, Guo Q, Ke Y, Yu M, Jin Y, Liu Y, Ding Q, Di D, Yang L, Xing G, Tian H, Jin C, Gao F, Friend R H, Wang J, Huang W. Perovskite light-emitting diodes based on solution-processed self-organized multiple quantum wells. Nature Photonics, 2016, 10(11): 699–704
61. Lim J, Park M, Bae W K, Lee D, Lee S, Lee C, Char K. Highly efficient cadmium-free quantum dot light-emitting diodes enabled by the direct formation of excitons within InP@ZnSeS quantum dots. ACS Nano, 2013, 7(10): 9019–9026
62. Tessier M D, Dupont D, De Nolf K D, Roo J D, Hens Z. Economic and size-tunable synthesis of InP/ZnE (E = S, Se) colloidal quantum dots. Chemistry of Materials, 2015, 27(13): 4893–4898
63. Kim J H, Yang H. High-efficiency Cu–In–S quantum-dot-light-emitting device exceeding 7%. Chemistry of Materials, 2016, 28 (17): 6329–6335
64. Bai Z, Ji W, Han D, Chen L, Chen B, Shen H, Zou B, Zhong H. Hydroxyl-terminated $CuInS_2$ based quantum dots: toward efficient and bright light emitting diodes. Chemistry of Materials, 2016, 28 (4): 1085–1091
65. Bol A A, Meijerink A. Luminescence quantum efficiency of nanocrystalline ZnS: Mn^{2+}. 1. Surface passivation and Mn^{2+} concentration. Journal of Physical Chemistry B, 2001, 105(42): 10197–10202
66. Shen H, Wang H, Li X, Niu J Z, Wang H, Chen X, Li L S. Phosphine-free synthesis of high quality ZnSe, ZnSe/ZnS, and Cu-, Mn-doped ZnSe nanocrystals. Dalton Transactions (Cambridge, England), 2009, (47): 10534–10540
67. Jurbergs D, Rogojina E, Mangolini L, Kortshagen U. Silicon nanocrystals with ensemble quantum yields exceeding 60%. Applied Physics Letters, 2006, 88(23): 233116
68. Cheng K Y, Anthony R, Kortshagen U R, Holmes R J. High-efficiency silicon nanocrystal light-emitting devices. Nano Letters, 2011, 11(5): 1952–1956
69. Zhang X, Zhang Y, Wang Y, Kalytchuk S, Kershaw S V, Wang Y, Wang P, Zhang T, Zhao Y, Zhang H, Cui T, Wang Y, Zhao J, Yu W W, Rogach A L. Color-switchable electroluminescence of carbon dot light-emitting diodes. ACS Nano, 2013, 7(12): 11234–11241
70. Yuan F, Wang Z, Li X, Li Y, Tan Z, Fan L, Yang S. Bright multicolor bandgap fluorescent carbon quantum dots for electroluminescent light-emitting diodes. Advanced Materials, 2017, 29 (3): 1604436
71. Song J, Li J, Li X, Xu L, Dong Y, Zeng H. Quantum dot light-emitting diodes based on inorganic perovskite cesium lead halides ($CsPbX_3$). Advanced Materials, 2015, 27(44): 7162–7167
72. Jellicoe T C, Richter J M, Glass H F J, Tabachnyk M, Brady R, Dutton S E, Rao A, Friend R H, Credgington D, Greenham N C, Böhm M L. Synthesis and optical properties of lead-free cesium tin

halide perovskite nanocrystals. Journal of the American Chemical Society, 2016, 138(9): 2941–2944
73. Yang B, Chen J, Hong F, Mao X, Zheng K, Yang S, Li Y, Pullerits T, Deng W, Han K. Lead-free, air-stable all-inorganic cesium bismuth halide perovskite nanocrystals. Angewandte Chemie International Edition, 2017, 56(41): 12471–12475
74. Chen Q, De Marco N, Yang Y M, Song T B, Chen C C, Zhao H, Hong Z, Zhou H, Yang Y. Under the spotlight: the organic–inorganic hybrid halide perovskite for optoelectronic applications. Nano Today, 2015, 10(3): 355–396
75. Cortecchia D, Dewi H A, Yin J, Bruno A, Chen S, Baikie T, Boix P P, Grätzel M, Mhaisalkar S, Soci C, Mathews N. Lead-free $MA_2CuCl_xBr_{4-x}$ hybrid perovskites. Inorganic Chemistry, 2016, 55(3): 1044–1052
76. Lee K H, Lee J H, Kang H D, Park B, Kwon Y, Ko H, Lee C, Lee J, Yang H. Over 40 cd/A efficient green quantum dot electroluminescent device comprising uniquely large-sized quantum dots. ACS Nano, 2014, 8(5): 4893–4901
77. Anikeeva P O, Halpert J E, Bawendi M G, Bulović V. Electroluminescence from a mixed red-green-blue colloidal quantum dot monolayer. Nano Letters, 2007, 7(8): 2196–2200
78. Bae W K, Lim J, Lee D, Park M, Lee H, Kwak J, Char K, Lee C, Lee S. R/G/B/natural white light thin colloidal quantum dot-based light-emitting devices. Advanced Materials, 2014, 26(37): 6387–6393
79. Dai X, Deng Y, Peng X, Jin Y. Quantum-dot light-emitting diodes for large-area displays: towards the dawn of commercialization. Advanced Materials, 2017, 29(14): 1607022
80. Li J, Xu L, Wang T, Song J, Chen J, Xue J, Dong Y, Cai B, Shan Q, Han B, Zeng H. 50-fold EQE improvement up to 6.27% of solution-processed all-inorganic perovskite $CsPbBr_3$ QLEDs via surface ligand density control. Advanced Materials, 2017, 29(5): 1603885
81. Dai X, Zhang Z, Jin Y, Niu Y, Cao H, Liang X, Chen L, Wang J, Peng X. Solution-processed, high-performance light-emitting diodes based on quantum dots. Nature, 2014, 515(7525): 96–99
82. Manders J R, Qian L, Titov A, Hyvonen J, Tokarz-Scott J, Acharya K P, Yang Y, Cao W, Zheng Y, Xue J, Holloway P H. High efficiency and ultra-wide color gamut quantum dot LEDs for next generation displays. Journal of the Society for Information Display, 2015, 23(11): 523–528
83. Shen H, Cao W, Shewmon N T, Yang C, Li L S, Xue J. High-efficiency, low turn-on voltage blue-violet quantum-dot-based light-emitting diodes. Nano Letters, 2015, 15(2): 1211–1216
84. Yang Y, Zheng Y, Cao W, Titov A, Hyvonen J, Manders J R, Xue J, Holloway P H, Qian L. High-efficiency light-emitting devices based on quantum dots with tailored nanostructures. Nature Photonics, 2015, 9(4): 259–266
85. Gao M, Li L, Song Y. Inkjet printing wearable electronic devices. Journal of Materials Chemistry C, Materials for Optical and Electronic Devices, 2017, 5(12): 2971–2993
86. Liu X, Tarn T J, Huang F, Fan J. Recent advances in inkjet printing synthesis of functional metal oxides. Particuology, 2015, 19: 1–13
87. Jang D, Kim D, Moon J. Influence of fluid physical properties on ink-jet printability. Langmuir, 2009, 25(5): 2629–2635
88. Liu H M, Zheng H, Xu W, Peng J B. Technology and development of ink-jet printing electroluminescence displays. Materials China, 2014, 33(3): 163–171
89. Deegan R D, Bakajin O, Dupont T F, Huber G, Nagel S R, Witten T A. Capillary flow as the cause of ring stains from dried liquid drops. Nature, 1997, 389(6653): 827–829
90. Yunker P J, Still T, Lohr M A, Yodh A G. Suppression of the coffee-ring effect by shape-dependent capillary interactions. Nature, 2011, 476(7360): 308–311
91. Soltman D, Subramanian V. Inkjet-printed line morphologies and temperature control of the coffee ring effect. Langmuir, 2008, 24 (5): 2224–2231
92. Hu H, Larson R G. Marangoni effect reverses coffee-ring depositions. Journal of Physical Chemistry B, 2006, 110(14): 7090–7094
93. Kim D, Jeong S, Park B K, Moon J. Direct writing of silver conductive patterns: improvement of film morphology and conductance by controlling solvent compositions. Applied Physics Letters, 2006, 89(26): 264101
94. Still T, Yunker P J, Yodh A G. Surfactant-induced Marangoni eddies alter the coffee-rings of evaporating colloidal drops. Langmuir, 2012, 28(11): 4984–4988
95. Jiang C, Zhong Z, Liu B, He Z, Zou J, Wang L, Wang J, Peng J, Cao Y. Coffee-ring-free quantum dot thin film using inkjet printing from a mixed-solvent system on modified ZnO transport layer for light-emitting devices. ACS Applied Materials & Interfaces, 2016, 8(39): 26162–26168
96. Cui Z. Printed Electronics: Materials, Technologies and Applications. Beijing: Higher Education Press, 2012 (in Chinese)
97. Shin P, Sung J. The effect of driving waveforms on droplet formation in a piezoelectric inkjet nozzle. In: Proceedings of Electronics Packaging Technology Conference, Singapore. IEEE, 2009, 158–162
98. Kwon K S, Kim W. A waveform design method for high-speed inkjet printing based on self-sensing measurement. Sensors and Actuators. A, Physical, 2007, 140(1): 75–83
99. Shin P, Sung J, Lee M H. Control of droplet formation for low viscosity fluid by double waveforms applied to a piezoelectric inkjet nozzle. Microelectronics and Reliability, 2011, 51(4): 797–804
100. Kwon K S. Experimental analysis of waveform effects on satellite and ligament behavior via *in situ* measurement of the drop-on-demand drop formation curve and the instantaneous jetting speed curve. Journal of Micromechanics and Microengineering, 2010, 20 (11): 115005
101. Kim C, Nogi M, Suganuma K, Yamato Y. Inkjet-printed lines with well-defined morphologies and low electrical resistance on repellent pore-structured polyimide films. ACS Applied Materials & Interfaces, 2012, 4(4): 2168–2173
102. Nguyen P Q M, Yeo L P, Lok B K, Lam Y C. Patterned surface with controllable wettability for inkjet printing of flexible printed electronics. ACS Applied Materials & Interfaces, 2014, 6(6): 4011–4016
103. Mahajan A, Hyun W J, Walker S B, Rojas G A, Choi J H, Lewis J A, Francis L F, Frisbie C D. A self-aligned strategy for printed

electronics: exploiting capillary flow on microstructured plastic surfaces. Advanced Electronic Materials, 2015, 1(9): 1500137

104. Park K S, Baek J, Park Y, Lee L, Lee Y E, Kang Y, Sung M M. Inkjet-assisted nanotransfer printing for large-scale integrated nanopatterns of various single-crystal organic materials. Advanced Materials, 2016, 28(15): 2874–2880
105. Wu S F, Li S H, Wang Y K, Huang C C, Sun Q, Liang J J, Liao L S, Fung M K. White organic LED with a luminous efficacy exceeding 100 $\mathrm{lm \cdot W^{-1}}$ without light out-coupling enhancement techniques. Advanced Functional Materials, 2017, 27(31): 1701314
106. Chiba T, Pu Y J, Kido J. Solution-processed white phosphorescent tandem organic light-emitting devices. Advanced Materials, 2015, 27(32): 4681–4687
107. Vaart N C V D, Lifka H, Budzelaar F P M, Rubingh J E J M, Hoppenbrouwers J J L, Dijksman J F, Verbeek R G F A, Woudenberg R, Vossen F J, Hiddink M G H, Rosink J J W M, Bernards T N M, Giraldo A. 44.4: distinguished paper: towards large-area full-color active-matrix printed polymer OLED television. Sid Symposium Digest of Technical Papers, 2004, 35(1): 1284–1287
108. Hebner T R, Wu C C, Marcy D, Lu M H, Sturm J C. Ink-jet printing of doped polymers for organic light emitting devices. Applied Physics Letters, 1998, 72(5): 519–521
109. Kobayashi H, Kanbe S, Seki S, Kigchi H, Kimura M, Yudasaka I, Miyashita S, Shimoda T, Towns C R, Burroughes J H, Friend R H. A novel RGB multicolor light-emitting polymer display. Synthetic Metals, 2000, 111–112: 125–128
110. Duineveld P C, de Kok M M, Buechel M, Sempel A, Mutsaers K A H, van de Weijer P, Camps I G J, van de Biggelaar T, Rubingh J E J M, Haskal E I. Ink-jet printing of polymer light-emitting devices. Proceedings of the Society for Photo-Instrumentation Engineers, 2002, 4464: 59–67
111. Fleuster M, Klein M, Roosmalen P, Wit A, Schwab H. 44.2: Mass manufacturing of full color passive-matrix and active-matrix PLED displays. SID Symposium Digest of Technical Papers, 2004, 35(1): 1276–1279
112. Gupta R, Ingle A, Natarajan S, So F. 44.3: Ink jet printed organic displays. SID Symposium Digest of Technical Papers, 2004, 35(1): 1281–1283
113. Rhee J, Wang J, Cha S, Chung J, Lee D, Hong S, Choi B, Goh J, Jung K, Kim S, Ko C, Koh B, Sung S, Park K, Kim N, Chung K, Gregory H, Bale M, Creighton C, Wild B, Shawcross A, Webb L, Hatcher M, Lees R, Richardson M, Bassett O, Coats S, Jongman J, Goddard S, Lyon P, Murphy C, Wallace P, Carte J, Athanassopoulou N. P-177: a 14.1-in. full-color polymer-LED display with a-Si TFT backplane by ink-jet printing. SID Symposium Digest of Technical Papers, 2006, 37(1): 895–897
114. Gohda T, Kobayashi Y, Okano K, Inoue S, Okamoto K, Hashimoto S, Yamamoto E, Morita H, Mitsui S, Koden M. 58.3: a 3.6-in. 202-ppi full-color AMPLED display fabricated by ink-jet method. SID Symposium Digest of Technical Papers, 2006, 37(1): 1767–1770
115. Takei S, Kitabayashi A, Hanaoka H, Shinohara K, Goto M, Nozawa T, Kubota T, Kasai T, Sakai S, Miyashita S. P-186L: late-news poster: fabrication of completely uniform OLED display using an improved inkjet method. SID Symposium Digest of Technical Papers, 2009, 40(1): 1351–1354
116. Zheng H, Zheng Y, Liu N, Ai N, Wang Q, Wu S, Zhou J, Hu D, Yu S, Han S, Xu W, Luo C, Meng Y, Jiang Z, Chen Y, Li D, Huang F, Wang J, Peng J, Cao Y. All-solution processed polymer light-emitting diode displays. Nature Communications, 2013, 4(3): 1971
117. Chen C, Chung Y, Chen C, Chen P Y, Lee C H, Cheng L I, Tsai L, Ting H C, Lin L F, Chen C C, Shih T H, Chen C Y, Chang L H, Lin Y. 55.2: ink-jet printed AMOLED displays based on high mobility IGZO TFTs: cost does matter! Sid Symposium Digest of Technical Papers, 2014, 44(1):760–762
118. Chen P Y, Chen C L, Chen C C, Tsai L, Ting H C, Lin L F, Chen C C, Chen C Y, Chang L H, Shih T H, Chen Y H, Huang J C, Lai M Y, Hsu C M, Lin Y. 30.1: invited paper: 65-inch inkjet printed organic light-emitting display panel with high degree of pixel uniformity. SID Symposium Digest of Technical Papers, 2014, 45 (1): 396–398
119. JOLED Inc. 世界初の印刷方式4K有　ELパネル、サンプル出荷を　始! (2017/ 5/17)
120. Olivier S, Derue L, Geffroy B, Ishow E, Maindron T. Inkjet printing of photopolymerizable small molecules for OLED applications. In: Proceedings of Organic Light Emitting Materials and Devices XIX. International Society for Optics and Photonics, 2015, 9566: 95661N
121. Haverinen H M, Myllylä R A, Jabbour G E. Inkjet printed RGB quantum dot-hybrid LED. Journal of Display Technology, 2010, 6 (3): 87–89
122. Kim T H, Cho K S, Lee E K, Lee S J, Chae J, Kim J W, Kim D H, Kwon J Y, Amaratunga G, Lee S Y, Choi B L, Kuk Y, Kim J M, Kim K. Full-colour quantum dot displays fabricated by transfer printing. Nature Photonics, 2011, 5(3): 176–182
123. Kim B H, Onses M S, Lim J B, Nam S, Oh N, Kim H, Yu K J, Lee J W, Kim J H, Kang S K, Lee C H, Lee J, Shin J H, Kim N H, Leal C, Shim M, Rogers J A. High-resolution patterns of quantum dots formed by electrohydrodynamic jet printing for light-emitting diodes. Nano Letters, 2015, 15(2): 969–973
124. Han J, Ko D, Park M, Roh J, Jung H, Lee Y, Kwon Y, Sohn J, Bae W K, Chin B D, Lee C. Toward high-resolution, inkjet-printed, quantum dot light-emitting diodes for next-generation displays. Journal of the Society for Information Display, 2016, 24(9): 545–551
125. Liu Y, Li F, Xie X, Chen W, Xu Z, Zheng C, Hu H, Guo T. P-122: red and green quantum dots light-emitting diodes fabricated by inkjet printing. Sid Symposium Digest of Technical Papers, 2017, 48(1): 1715–1718
126. Jiang C, Mu L, Zou J, He Z, Zhong Z, Wang LMiao, Xu, Wang J, Peng J, Cao Y.Full-color quantum dots active matrix display fabricated by ink-jet printing. Science China Chemistry, 2017, https://doi.org/10.1007/s11426-017-9087-y
127. Xia S, Cheon K O, Brooks J J, Rothman M, Ngo T, Hett P, Kwong R C, Inbasekaran M, Brown J J, Sonoyama T, Ito M, Seki S, Miyashita S. Printable phosphorescent organic light-emitting devices. Journal of the Society for Information Display, 2009, 17 (2): 167–172

128. Chen P, Chen C, Hsieh C, Lin J M, Lin Y S, Lin Y. P-56: High resolution organic light-emitting diode panel fabricated by ink jet printing process. Sid Symposium Digest of Technical Papers, 2015, 46(1):1352–1354
129. Sax S, Rugen-Penkalla N, Neuhold A, Schuh S, Zojer E, List E J W, Müllen K. Efficient blue-light-emitting polymer heterostructure devices: the fabrication of multilayer structures from orthogonal solvents. Advanced Materials, 2010, 22(18): 2087–2091
130. Patel D G D, Graham K R, Reynolds J R. A Diels–Alder crosslinkable host polymer for improved PLED performance: the impact on solution processed doped device and multilayer device performance. Journal of Materials Chemistry, 2012, 22(7): 3004–3014
131. Kim J S, Ho P K H, Murphy C E, Friend R H. Phase separation in polyfluorene-based conjugated polymer blends: lateral and vertical analysis of blend spin-cast thin films. Macromolecules, 2004, 37 (8): 2861–2871
132. Xia Y, Friend R H. Controlled phase separation of polyfluorene blends via inkjet printing. Macromolecules, 2005, 38(15): 6466–6471
133. Chang S C, Liu J, Bharathan J, Yang Y, Onohara H, Kido J. Multicolor organic light-emitting diodes processed by hybrid inkjet printing. Advanced Materials, 1999, 11(9): 734–737
134. Gorter H, Coenen M J J, Slaats M W L, Ren M, Lu W, Kuijpers C J, Groen W A. Toward inkjet printing of small molecule organic light emitting diodes. Thin Solid Films, 2013, 532: 11–15
135. Ding Z, Xing R, Fu Q, Ma D, Han Y. Patterning of pinhole free small molecular organic light-emitting films by ink-jet printing. Organic Electronics, 2011, 12(4): 703–709
136. Coe S, Woo W K, Bawendi M, Bulović V. Electroluminescence from single monolayers of nanocrystals in molecular organic devices. Nature, 2002, 420(6917): 800–803
137. Kim H H, Park S, Yi Y , Son D I, Park C, Hwang D K, Choi W K. Inverted quantum dot light emitting diodes using polyethylenimine ethoxylated modified ZnO. Scientific Reports, 2015, 5: 8968
138. Kim O S, Kang B H, Lee J S, Lee S W, Cha S H, Lee J W, Kim S W, Kim S H, Kang S W. Efficient quantum dots light-emitting devices using polyvinyl pyrrolidone-capped ZnO nanoparticles with enhanced charge transport. IEEE Electron Device Letters, 2016, 37(8): 1022–1024
139. Liang F, Liu Y, Hu Y, Shi Y L, Liu Y Q, Wang Z K, Wang X D, Sun B Q, Liao L S. Polymer as an additive in the emitting layer for high-performance quantum dot light-emitting diodes. ACS Applied Materials & Interfaces, 2017, 9(23): 20239–20246
140. Kim L, Anikeeva P O, Coe-Sullivan S A, Steckel J S, Bawendi M G, Bulović V. Contact printing of quantum dot light-emitting devices. Nano Letters, 2008, 8(12): 4513–4517
141. Kim B H, Nam S, Oh N, Cho S Y, Yu K J, Lee C H, Zhang J, Deshpande K, Trefonas P, Kim J H, Lee J, Shin J H, Yu Y, Lim J B, Won S M, Cho Y K, Kim N H, Seo K J, Lee H, Kim T I, Shim M, Rogers J A. Multilayer transfer printing for pixelated, multicolor quantum dot light-emitting diodes. ACS Nano, 2016, 10(5): 4920–4925
142. Choi M K, Yang J, Kang K, Kim D C, Choi C, Park C, Kim S J, Chae S I, Kim T H, Kim J H, Hyeon T, Kim D H. Wearable red-green-blue quantum dot light-emitting diode array using high-resolution intaglio transfer printing. Nature Communications, 2015, 6: 7149
143. Roy D, Munz M, Colombi P, Bhattacharyya S, Salvetat J P, Cumpson P J, Saboungi M L. Directly writing with nanoparticles at the nanoscale using dip-pen nanolithography. Applied Surface Science, 2007, 254(5): 1394–1398
144. Gokarna A, Lee S K, Hwang J S, Cho Y H, Lim Y T, Chung B H, Lee M. Fabrication of CdSe/ZnS quantum-dot-conjugated protein microarrays and nanoarrays. Journal of the Korean Physical Society, 2008, 53(925): 3047–3050
145. Park J S, Kyhm J, Kim H H, Jeong S, Kang J, Lee S E, Lee K T, Park K, Barange N, Han J, Song J D, Choi W K, Han I K. Alternative patterning process for realization of large-area, full-color, active quantum dot display. Nano Letters, 2016, 16(11): 6946–6953
146. Haverinen H M, Myllylä R A, Jabbour G E. Inkjet printing of light emitting quantum dots. Applied Physics Letters, 2009, 94(7): 073108

Luhua Lan received his B.S. degree in Information Display and Opto-Electronic technology from South China University of Technology, Guangzhou, China, in 2016. He is currently working toward his M.S. degree in Materials Physics and Chemistry in South China University of Technology, Guangzhou, China. His current research interests include interface optimization of OLEDs and QLEDs fabricated by solotion processing.

Jianhua Zou is currently an Associate Research Fellow (2013) in the School of Material Science and Engineering at South China University of Technology (SCUT). He received his Bachelors degree in Materials Physics from North East University (China) in 2005, and his Ph.D. degree from the Physics Department at SCUT in 2010. His current research interests is device physics in organic electronics, including OLEDs and QLED. He has also published more than 50 papers on high-impact journals in these topics.

Congbiao Jiang received his B.S. degree in Material Physics from Wuhan University of Science and Technology, Wuhan, China, in 2014. He is currently working toward his Ph.D. degree in Materials Physics and Chemistry in South China University of Technology, Guangzhou, China. His current research interests include photoelectric materials, technique optimization on inkjet printed electroluminescent decives and physics of device.

Lei Wang received his B.S. degree in the department of Polymer Materials Science and Engineering from Hebei University of Technology in 2004, and his Ph.D. degree in Materials Physics from South China University of Technology (SCUT) in 2009. He is currently an Associate Research Fellow (2011) in the SCUT. His research interests include organic and inorganic semiconductor materials, devices and their process development, and he has done a large number of scientific research work in the field of OLED and metal oxide TFT.

Junbiao Peng received his B.S. degree in Physics at Jilin University in 1984 and M.S. and Ph.D. degrees respectively in 1987 and 1993 in Changchun Institute of Physics (CIP), Chinese Academy of Sciences. In the subsequent years, he did his postdoc work in the Korea Institute of Science and Technology and the National Institute of Materials and Chemical Research (NIMC), Japan. In 2001, he joined the Institute of Polymer Optoelectronic Materials and Devices, South China University of Technology, as a full professor. His current research interests include design, characterization, and application of organic optoelectronic devices such as OLEDs, OPVs and TFTs.